

Semileptonic Kaon Decays

J. Bijnens¹, **G. Colangelo**^{2,3}, **G. Ecker**⁴ and **J. Gasser**²

¹) Nordita, Blegdamsvej 17, DK-2000 Copenhagen

²) Inst. Theor. Physik, Univ. Bern, Sidlerstrasse 5, CH-3012 Bern

³) Dipartimento di Fisica, Università di Roma II - "Tor Vergata"

Via della Ricerca Scientifica 1, I-00173 Roma

⁴) Inst. Theor. Physik, Univ. Wien, Boltzmanngasse 5, A-1090 Wien

Contents

1	Radiative K_{l2} decays	318
1.1	Matrix elements and kinematics	318
1.2	Decay rates	319
1.3	Determination of $A(W^2)$ and $V(W^2)$	321
1.4	Previous experiments	324
1.5	Theory	325
1.6	Comment on tensor couplings	327
1.7	Improvements at DAΦNE	329
2	The decays $K^\pm \rightarrow l^\pm \nu l'^+ l'^-$	329
2.1	Matrix elements	329
2.2	Decay distributions	330

¹Supported by the INFN, by the EC under the HCM contract number CHRX-CT920026 and by the authors home institutions

2.3	Theory	331
2.4	Numerical results	332
2.5	Present experimental status	334
2.6	Improvements at DAΦNE	334
3	K_{l3} decays	335
3.1	Matrix elements and kinematics	335
3.2	Decay rates	336
3.3	Determination of the K_{l3} form factors	337
3.4	Previous measurements	338
3.5	Theory	339
3.6	Comment on tensor couplings	343
3.7	Improvements at DAΦNE	344
4	Radiative K_{l3} decays	344
4.1	Matrix elements	344
4.2	Decay rates	347
4.3	Previous experiments	348
4.4	Theory	349
4.5	Improvements at DAΦNE	354
5	K_{l4} decays	354
5.1	Kinematics	354
5.2	Matrix elements	356
5.3	Decay rates	357
5.4	Isospin decomposition	359
5.5	Partial wave expansion	360
5.6	Previous experiments	361
5.7	Theory	364
5.8	Determination of L_1, L_2 and L_3	370
5.9	Predictions	373
5.10	Improvements at DAΦNE	375
6	K_{e5} decays	377
6.1	Matrix elements and decay rates	377

6.2	Previous experiments	377
6.3	Theory	378
6.4	Improvements at DAΦNE	378

Bibliography	385
---------------------	------------

Note:

- The number of events quoted for DAΦNE are based on a luminosity of $5 \cdot 10^{32} \text{ cm}^{-2} \text{ s}^{-1}$, which is equivalent [1] to an annual rate of $9 \cdot 10^9$ ($1.1 \cdot 10^9$) tagged K^\pm (K_L) (1 year = 10^7 s assumed).
- Whenever we quote a branching ratio for a semileptonic K^0 decay, it stands for the branching ratio of the corresponding K_L decay, e.g.,

$$BR(K^0 \rightarrow \pi^- l^+ \nu) \equiv BR(K_L \rightarrow \pi^\pm l^\mp \nu) .$$

- We use the data from the Particle Data Group edition 1990 [3] throughout. Please contact one of the authors in case that very high precision is needed for a particular matrix element. We would then convert the relevant quantity to the newest data compilation available.
- If not stated explicitly, we always use for the low-energy constants L_1, \dots, L_{10} the values displayed in table 1 in ref. [2].
- More notation is provided in appendix A.

1 Radiative K_{l2} decays

We consider the $K_{l2\gamma}$ decay

$$K^+(p) \rightarrow l^+(p_l)\nu_l(p_\nu)\gamma(q) \quad [K_{l2\gamma}] \quad (1.1)$$

where l stands for e or μ , and γ is a real photon with $q^2 = 0$. Processes where the (virtual) photon converts into a e^+e^- or $\mu^+\mu^-$ pair are considered in the next subsection. The K^- mode is obtained from (1.1) by charge conjugation.

1.1 Matrix elements and kinematics

The matrix element for $K^+ \rightarrow l^+\nu_l\gamma$ has the structure

$$T = -iG_F e V_{us}^* \epsilon_\mu^* \{F_K L^\mu - H^{\mu\nu} l_\nu\} \quad (1.2)$$

with

$$\begin{aligned} L^\mu &= m_l \bar{u}(p_\nu)(1 + \gamma_5) \left(\frac{2p^\mu}{2pq} - \frac{2p_l^\mu + \not{q}\gamma^\mu}{2p_l q} \right) v(p_l) \\ l^\mu &= \bar{u}(p_\nu)\gamma^\mu(1 - \gamma_5)v(p_l) \\ H^{\mu\nu} &= iV(W^2)\epsilon^{\mu\nu\alpha\beta}q_\alpha p_\beta - A(W^2)(qWg^{\mu\nu} - W^\mu q^\nu) \\ W^\mu &= (p - q)^\mu = (p_l + p_\nu)^\mu. \end{aligned} \quad (1.3)$$

Here, ϵ_μ denotes the polarization vector of the photon with $q^\mu \epsilon_\mu = 0$, whereas A, V stand for two Lorentz invariant amplitudes which occur in the general decomposition of the tensors

$$I^{\mu\nu} = \int dx e^{iqx+iWy} \langle 0 | TV_{em}^\mu(x) I_{4-i5}^\nu(y) | K^+(p) \rangle, \quad I = V, A. \quad (1.4)$$

The form factor A (V) is related to the matrix element of the axial (vector) current in (1.4). In appendix C we display the general decomposition of $A^{\mu\nu}$, $V^{\mu\nu}$ for $q^2 \neq 0$ and provide also the link with the notation used by the PDG [3] and in [4, 5].

The term proportional to L^μ in (1.2) does not contain unknown quantities – it is determined by the amplitude of the nonradiative decay $K^+ \rightarrow l^+\nu_l$. This part of the amplitude is usually referred to as “inner Bremsstrahlung (IB) contribution”, whereas the term proportional to $H^{\mu\nu}$ is called “structure dependent (SD) part”.

The form factors are analytic functions in the complex W^2 -plane cut along the positive real axis. The cut starts at $W^2 = (M_K + 2M_\pi)^2$ for A (at $W^2 = (M_K + M_\pi)^2$ for V). In our phase convention, A and V are real in the physical region of $K_{l2\gamma}$ decays,

$$m_l^2 \leq W^2 \leq M_K^2. \quad (1.5)$$

The kinematics of (spin averaged) $K_{l2\gamma}$ decays needs two variables, for which we choose the conventional quantities

$$x = 2pq/M_K^2 \quad , \quad y = 2pp_l/M_K^2 \quad . \quad (1.6)$$

In the K rest frame, the variable x (y) is proportional to the photon (charged lepton) energy,

$$x = 2E_\gamma/M_K \quad , \quad y = 2E_l/M_K \quad , \quad (1.7)$$

and the angle $\theta_{l\gamma}$ between the photon and the charged lepton is related to x and y by

$$x = \frac{(1 - y/2 + A/2)(1 - y/2 - A/2)}{1 - y/2 + A/2 \cos \theta_{l\gamma}} \quad ; \quad A = \sqrt{y^2 - 4r_l} \quad . \quad (1.8)$$

In terms of these quantities, one has

$$W^2 = M_K^2(1 - x) \quad ; \quad (q^2 = 0) \quad . \quad (1.9)$$

We write the physical region for x and y as

$$\begin{aligned} 2\sqrt{r_l} &\leq y \leq 1 + r_l \\ 1 - \frac{1}{2}(y + A) &\leq x \leq 1 - \frac{1}{2}(y - A) \end{aligned} \quad (1.10)$$

or, equivalently, as

$$\begin{aligned} 0 &\leq x \leq 1 - r_l \\ 1 - x + \frac{r_l}{(1 - x)} &\leq y \leq 1 + r_l \end{aligned} \quad (1.11)$$

where

$$r_l = m_l^2/M_K^2 = \begin{cases} 1.1 \cdot 10^{-6} (l = e) \\ 4.6 \cdot 10^{-2} (l = \mu) \end{cases} \quad . \quad (1.12)$$

1.2 Decay rates

The partial decay rate is

$$d\Gamma = \frac{1}{2M_K(2\pi)^5} \sum_{spins} |T|^2 d_{LIPS}(p; p_l, p_\nu, q). \quad (1.13)$$

The Dalitz plot density

$$\rho(x, y) = \frac{d^2\Gamma}{dx dy} = \frac{M_K}{256\pi^3} \sum_{spins} |T|^2 \quad (1.14)$$

is a Lorentz invariant function which contains V and A in the following form [6],

$$\begin{aligned}
\rho(x, y) &= \rho_{\text{IB}}(x, y) + \rho_{\text{SD}}(x, y) + \rho_{\text{INT}}(x, y) \\
\rho_{\text{IB}}(x, y) &= A_{\text{IB}} f_{\text{IB}}(x, y) \\
\rho_{\text{SD}}(x, y) &= A_{\text{SD}} M_K^2 \left[(V + A)^2 f_{\text{SD}+}(x, y) + (V - A)^2 f_{\text{SD}-}(x, y) \right] \\
\rho_{\text{INT}}(x, y) &= A_{\text{INT}} M_K \left[(V + A) f_{\text{INT}+}(x, y) + (V - A) f_{\text{INT}-}(x, y) \right]
\end{aligned} \tag{1.15}$$

where

$$\begin{aligned}
f_{\text{IB}}(x, y) &= \left[\frac{1 - y + r_l}{x^2(x + y - 1 - r_l)} \right] \left[x^2 + 2(1 - x)(1 - r_l) - \frac{2xr_l(1 - r_l)}{x + y - 1 - r_l} \right] \\
f_{\text{SD}+}(x, y) &= [x + y - 1 - r_l] [(x + y - 1)(1 - x) - r_l] \\
f_{\text{SD}-}(x, y) &= [1 - y + r_l] [(1 - x)(1 - y) + r_l] \\
f_{\text{INT}+}(x, y) &= \left[\frac{1 - y + r_l}{x(x + y - 1 - r_l)} \right] [(1 - x)(1 - x - y) + r_l] \\
f_{\text{INT}-}(x, y) &= \left[\frac{1 - y + r_l}{x(x + y - 1 - r_l)} \right] [x^2 - (1 - x)(1 - x - y) - r_l]
\end{aligned} \tag{1.16}$$

and

$$\begin{aligned}
A_{\text{IB}} &= 4r_l \left(\frac{F_K}{M_K} \right)^2 A_{\text{SD}} \\
A_{\text{SD}} &= \frac{G_F^2 |V_{us}|^2 \alpha}{32\pi^2} M_K^5 \\
A_{\text{INT}} &= 4r_l \left(\frac{F_K}{M_K} \right) A_{\text{SD}} .
\end{aligned} \tag{1.17}$$

For later convenience, we note that

$$A_{\text{SD}} = \frac{\alpha}{8\pi} \frac{1}{r_l(1 - r_l)^2} \left(\frac{M_K}{F_K} \right)^2 \Gamma(K \rightarrow l\nu_l) . \tag{1.18}$$

The indices IB, SD and INT stand respectively for the contribution from inner Bremsstrahlung, from the structure dependent part and from the interference term between the IB and the SD part in the amplitude.

To get a feeling for the magnitude of the various contributions IB, SD^\pm and INT^\pm to the decay rate, we consider the integrated rates

$$\Gamma_I = \int_{R_I} dx dy \rho_I(x, y) ; \quad I = \text{SD}^\pm, \text{INT}^\pm, \text{IB} , \tag{1.19}$$

where $\rho_{\text{SD}} = \rho_{\text{SD}+} + \rho_{\text{SD}-}$ etc. For the region R_I we take the full phase space for $I \neq \text{IB}$, and

$$R_{\text{IB}} = 214.5 \text{ MeV}/c \leq p_l \leq 231.5 \text{ MeV}/c . \tag{1.20}$$

Table 1.1: The quantities X_I, N_I . SD^\pm and INT^\pm are evaluated with full phase space, IB with restricted kinematics (1.20).

	SD^+	SD^-	INT^+	INT^-	IB	
X_I	$1.67 \cdot 10^{-2}$	$1.67 \cdot 10^{-2}$	$-8.22 \cdot 10^{-8}$	$3.67 \cdot 10^{-6}$	$3.58 \cdot 10^{-6}$	$K_{e2\gamma}$
X_I	$1.18 \cdot 10^{-2}$	$1.18 \cdot 10^{-2}$	$-1.78 \cdot 10^{-3}$	$1.23 \cdot 10^{-2}$	$3.68 \cdot 10^{-2}$	$K_{\mu2\gamma}$
N_I	2	2	1	1	0	

for the Bremsstrahlung contribution. Here p_l stands for the modulus of the lepton three momentum in the kaon rest system ². We consider constant form factors V, A and write for the rates and for the corresponding branching ratios

$$\begin{aligned}\Gamma_I &= A_{\text{SD}} \{M_K(V \pm A)\}^{N_I} X_I \\ \text{BR}_I &\doteq \Gamma_I / \Gamma_{\text{tot}} = N \{M_K(V \pm A)\}^{N_I} X_I\end{aligned}\quad (1.21)$$

with

$$N = A_{\text{SD}} / \Gamma_{\text{tot}} = 8.348 \cdot 10^{-2}. \quad (1.22)$$

The values for N_I and X_I are listed in table 1.1.

To estimate Γ_I and BR_I , we note that the form factors V, A are of order

$$M_K(V + A) \simeq -10^{-1} \quad , \quad M_K(V - A) \simeq -4 \cdot 10^{-2} \quad . \quad (1.23)$$

From this and from the entries in the table one concludes that for the above regions R_I , the interference terms INT^\pm are negligible in $K_{e2\gamma}$, whereas they are important in $K_{\mu2\gamma}$. Furthermore, IB is negligible for $K_{e2\gamma}$, because it is helicity suppressed as can be seen from the factor m_l^2 in A_{IB} . This term dominates however in $K_{\mu2\gamma}$.

1.3 Determination of $A(W^2)$ and $V(W^2)$

The decay rate contains two real functions

$$F^\pm(W^2) = V(W^2) \pm A(W^2) \quad (1.24)$$

as the only unknowns. In Figs. (1.1,1.2) we display contour plots for the density distributions $f_{\text{IB}}, \dots, f_{\text{INT}^\pm}$ for $l = \mu, e$. These five terms have obviously very different Dalitz plots. Therefore, in principle, one can determine the strength of each term by choosing a suitable kinematical region of observation. To pin down F^\pm , it would be sufficient to measure at each photon energy the interference term INT^\pm . This has not yet been achieved so far,

²This cut has been used in [5] for $K_{\mu2\gamma}$, because this kinematical region is free from $K_{\mu3}$ background. We apply it here for illustration also to the electron mode $K_{e2\gamma}$.

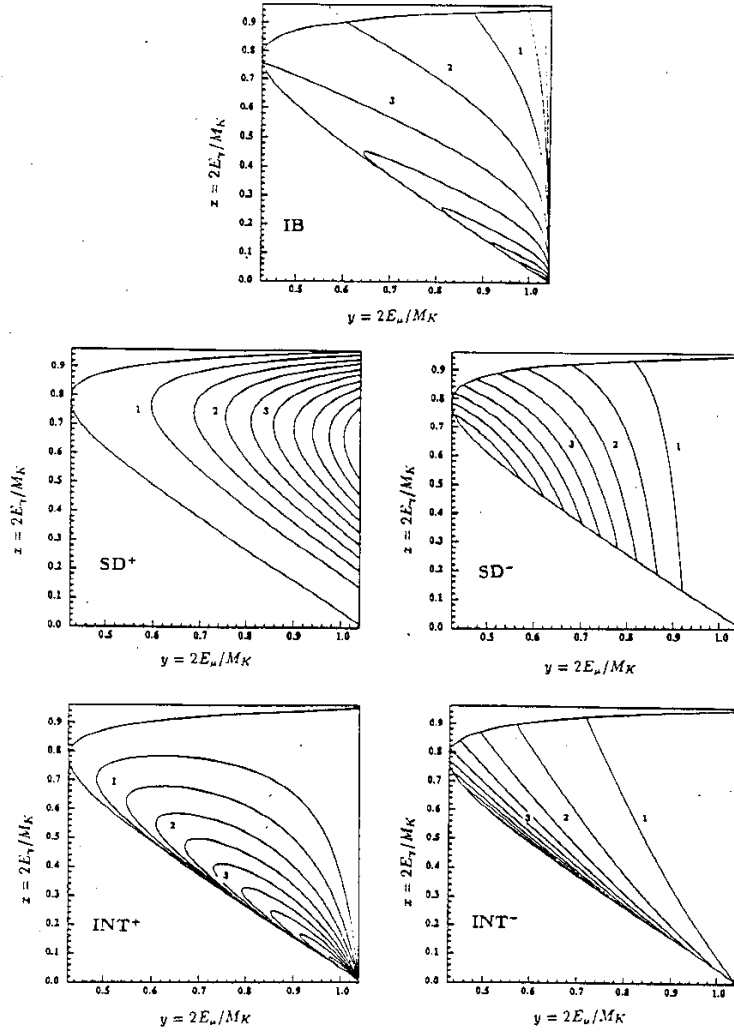


Figure 1.1: Contour plots for $f_{\text{IB}}, \dots, f_{\text{INT}\pm} [K_{\mu 2\gamma}]$. The numbering on the lines points towards increasing modulus. The normalization is arbitrary.

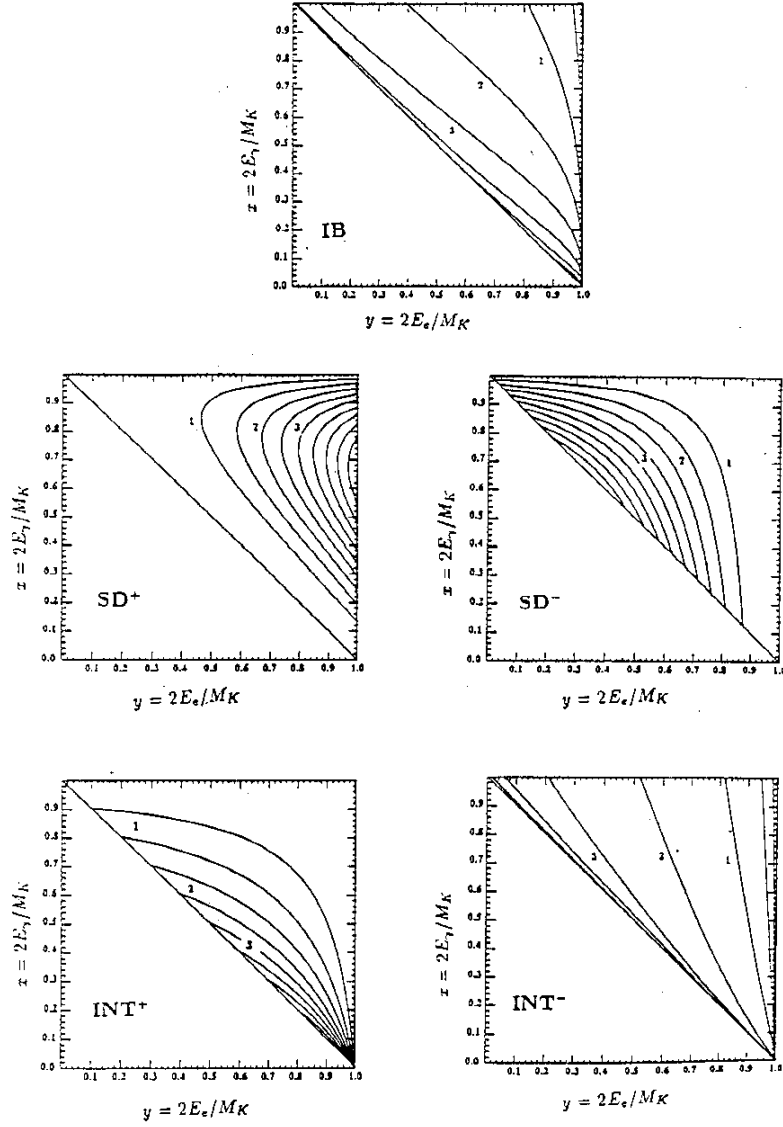


Figure 1.2: Contour plots for $f_{IB}, \dots, f_{INT\pm} [K_{e2\gamma}]$. The numbering on the lines points towards increasing modulus. The normalization is arbitrary.

either because the contribution of INT^\pm is too small (in $K_{e2\gamma}$), or because too few events have been collected (in $K_{\mu2\gamma}$). On the other hand, from a measurement of SD^\pm alone one can determine A, V only up to a fourfold ambiguity:

$$\text{SD}^\pm \rightarrow \{(V, A); -(V, A); (A, V); -(A, V)\}. \quad (1.25)$$

In terms of the ratio

$$\gamma_K = A/V \quad (1.26)$$

this ambiguity amounts to

$$\text{SD}^\pm \rightarrow \{\gamma_K; 1/\gamma_K\}. \quad (1.27)$$

Therefore, in order to pin down the amplitudes A and V uniquely, one must measure the interference terms INT^\pm as well.

1.4 Previous experiments

$K^+ \rightarrow e^+ \nu_e \gamma$

The PDG uses data from two experiments [4, 7], both of which have been sensitive mainly to the SD^+ term in (1.15). In [7], 56 events with $E_\gamma > 100$ MeV, $E_{e^+} > 236$ MeV and $\theta_{e^+\gamma} > 120^\circ$ have been identified, whereas the later experiment [4] has collected 51 events with $E_\gamma > 48$ MeV, $E_{e^+} > 235$ MeV and $\theta_{e^+\gamma} > 140^\circ$. In these kinematical regions, background from $K^+ \rightarrow e^+ \nu_e \pi^0$ is absent because $E_e^{\text{max}}(K_{e3}) = 228$ MeV. The combined result of both experiments is ³ [4]

$$\Gamma(\text{SD}^+)/\Gamma(K_{\mu2}) = (2.4 \pm 0.36) \cdot 10^{-5}. \quad (1.28)$$

For SD^- , the bound

$$\Gamma(\text{SD}^-)/\Gamma_{\text{total}} < 1.6 \cdot 10^{-4} \quad (1.29)$$

has been obtained from a sample of electrons with energies $220 \text{ MeV} \leq E_e \leq 230 \text{ MeV}$ [4]. Using (1.21, 1.22), the result (1.28) leads to

$$M_K |V + A| = 0.105 \pm 0.008. \quad (1.30)$$

The bound (1.29) on the other hand implies [4]

$$|V - A| / |V + A| < \sqrt{11}, \quad (1.31)$$

from where one concludes [4] that γ_K is outside the range -1.86 to -0.54 ,

$$\gamma_K \notin [-1.86, -0.54]. \quad (1.32)$$

³In all four experiments [7, 4, 5, 8] discussed here and below, the form factors A and V have been treated as constants.

Table 1.2: Measured branching ratios $\Gamma(K \rightarrow l\nu_l\gamma)/\Gamma_{\text{total}}$. The $K_{e2\gamma}$ data are from [7, 4], the $K_{\mu2\gamma}$ data from [5, 8]. The last column corresponds [5] to the cut (1.20).

	SD^+	SD^-	INT^+	$\text{SD}^- + \text{INT}^-$	total
$K_{e2\gamma}$	$(1.52 \pm 0.23) \cdot 10^{-5}$	$< 1.6 \cdot 10^{-4}$			
$K_{\mu2\gamma}$	$< 3 \cdot 10^{-5}$		$< 2.7 \cdot 10^{-5}$ (modulus)	$< 2.6 \cdot 10^{-4}$ (modulus)	$(3.02 \pm 0.10) \cdot 10^{-3}$

As we already mentioned, the interference terms INT^\pm in $K \rightarrow e\nu_e\gamma$ are small and can hardly ever be measured. As a result of this, the amplitudes A, V and the ratio γ_K determined from $K_{e2\gamma}$ are subject to the ambiguities (1.25), (1.27).

$$\underline{K^+ \rightarrow \mu^+ \nu_\mu \gamma}$$

Here, the interference terms INT^\pm are nonnegligible in appropriate regions of phase space (see Figs. (1.1,1.2)). Therefore, this decay allows one in principle to pin down V and A . The PDG uses data from two experiments [5, 8]. In [5], the momentum spectrum of the muon was measured in the region (1.20). In total 2 ± 3.44 SD^+ events have been found with $216 \text{ MeV}/c < p_\mu < 230 \text{ MeV}/c$ and $E_\gamma > 100 \text{ MeV}$, which leads to

$$M_K \mid V + A \mid < 0.16 \quad . \quad (1.33)$$

In order to identify the effect of the SD^- terms, the region $120 \text{ MeV}/c < p_\mu < 150 \text{ MeV}/c$ was searched. Here, the background from $K_{\mu3}$ decays was very serious. The authors found 142 $K_{\mu\nu\gamma}$ candidates and conclude that

$$-1.77 < M_K(V - A) < 0.21. \quad (1.34)$$

The result (1.33) is consistent with (1.30), and the bound (1.34) is worse than the result (1.31) obtained from $K_{e2\gamma}$. The branching ratios which follow [5] from (1.33,1.34) are displayed in table 1.2, where we also show the $K_{e2\gamma}$ results [7, 4]. The entry $\text{SD}^- + \text{INT}^-$ for $K_{\mu2\gamma}$ is based on additional constraints from $K_{e2\gamma}$ [5].

1.5 Theory

The amplitudes $A(W^2)$ and $V(W^2)$ have been worked out in the framework of various approaches, viz., current algebra, PCAC, resonance exchange, dispersion relations, For a rather detailed review together with an extensive list of references up to 1976 see [9]. Here, we concentrate on the predictions of V, A in the framework of CHPT.

1.5.1 Chiral expansion to one loop

The amplitudes A and V have been evaluated [10, 11] in the framework of CHPT to one loop. At leading order in the low-energy expansion, one has

$$A = V = 0. \quad (1.35)$$

As a consequence of this, the rate is entirely given by the IB contribution at leading order. At the one-loop level, one finds

$$\begin{aligned} A &= -\frac{4}{F}(L_9^r + L_{10}^r) \\ V &= -\frac{1}{8\pi^2} \frac{1}{F} \\ \gamma_K &= 32\pi^2(L_9^r + L_{10}^r), \end{aligned} \quad (1.36)$$

where L_9^r and L_{10}^r are the renormalized low-energy couplings evaluated at the scale μ (the combination $L_9^r + L_{10}^r$ is scale independent). The vector form factor stems from the Wess-Zumino term [12] which enters the low-energy expansion at order p^4 , see Ref. [2].

Remarks:

- (i) At this order in the low-energy expansion, the form factors A, V do not exhibit any W^2 -dependence. A nontrivial W^2 -dependence only occurs at the next order in the energy expansion (two-loop effect, see the discussion below). Note that the available analyses of experimental data of $K \rightarrow l\nu_l\gamma$ decays [7, 4, 5, 8] use constant form factors throughout.
- (ii) Once the combination $L_9 + L_{10}$ has been pinned down from other processes, Eq. (1.36) allows one to evaluate A, V unambiguously at this order in the low-energy expansion. Using $L_9 + L_{10} = 1.4 \cdot 10^{-3}$ and $F = F_\pi$, one has

$$\begin{aligned} M_K(A + V) &= -0.097 \\ M_K(V - A) &= -0.037 \\ \gamma_K &= 0.45. \end{aligned} \quad (1.37)$$

The result for the combination $(A + V)$ agrees with (1.30) within the errors, while γ_K is consistent with (1.32).

We display in table 1.3 the branching ratios BR_I (1.21) which follow from the prediction (1.37). These predictions satisfy of course the inequalities found from experimental data (see table 1.2).

Table 1.3: Chiral prediction at order p^4 for the branching ratios $\Gamma(K \rightarrow l\nu_l\gamma)/\Gamma_{\text{total}}$. The cut used in the last column is given in Eq. (1.20).

	SD ⁺	SD ⁻	INT ⁺	INT ⁻	total
$K_{e2\gamma}$	$1.30 \cdot 10^{-5}$	$1.95 \cdot 10^{-6}$	$6.64 \cdot 10^{-10}$	$-1.15 \cdot 10^{-8}$	$2.34 \cdot 10^{-6}$
$K_{\mu2\gamma}$	$9.24 \cdot 10^{-6}$	$1.38 \cdot 10^{-6}$	$1.44 \cdot 10^{-5}$	$-3.83 \cdot 10^{-5}$	$3.08 \cdot 10^{-3}$

1.5.2 W^2 -dependence of the form factors

The chiral prediction gives constant form factors at order p^4 . Terms of order p^6 have not yet been calculated. They would, however, generate a nontrivial W^2 - dependence both in V and A . In order to estimate the magnitude of these corrections, we consider one class of p^6 - contributions: terms which are generated by vector and axial-vector resonance exchange with strangeness [9, 13],

$$V(W^2) = \frac{V}{1 - W^2/M_{K^*}^2} \quad , \quad A(W^2) = \frac{A}{1 - W^2/M_{K_1}^2} \quad (1.38)$$

where V, A are given in (1.36). We now examine the effect of the denominators in (1.38) in the region $y \geq 0.95, x \geq 0.2$ which has been explored in $K^+ \rightarrow e^+\nu_e\gamma$ [4]. We put $m_e = 0$ and evaluate the rate

$$\frac{dP(x)}{dx} = \frac{N_{\text{tot}}}{\Gamma_{\text{tot}}} \int_{y=0.95}^1 \rho_{\text{SD}^+}(x, y) dy \quad (1.39)$$

where N_{tot} denotes the total number of K^+ decays considered, and $\Gamma_{\text{tot}}^{-1} = 1.24 \cdot 10^{-8}$ sec.

The function $\frac{dP(x)}{dx}$ is displayed in Fig. (1.3) for three different values of M_{K^*} and M_{K_1} , with $N_{\text{tot}} = 9 \cdot 10^9$. The total number of events

$$N_P = \int_{x=0.2}^1 dP(x) \quad (1.40)$$

is also indicated in each case. The difference between the dashed and the dotted line shows that the nearby singularity in the anomaly form factor influences the decay rate substantially at low photon energies. The effect disappears at $x \rightarrow 1$, where $W^2 = M_K^2(1 - x) \rightarrow 0$. To minimize the effect of resonance exchange, the large- x region should thus be considered. The low- x region, on the other hand, may be used to explore the W^2 -dependence of V and of A . For a rather exhaustive discussion of the relevance of this W^2 - dependence for the analysis of $K_{l2\gamma}$ decays we refer the reader to Ref. [9].

1.6 Comment on tensor couplings

Bolotov et al. [14] have analyzed radiative pion decays $\pi^- \rightarrow e^- \bar{\nu}_e \gamma$ in flight ($\simeq 80$ events) in a wider kinematical region than was explored in the high-statistics experiment of Bay et

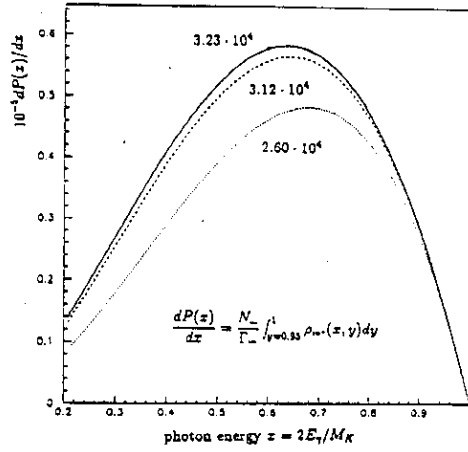


Figure 1.3: The rate $dP(x)/dx$ in (1.39), evaluated with the form factors (1.38) and $N_{\text{tot}} = 9 \cdot 10^9$. The solid line corresponds to $M_{K^*} = 890$ MeV, $M_{K_1} = 1.3$ GeV. The dashed line is evaluated with $M_{K^*} = 890$ MeV, $M_{K_1} = \infty$ and the dotted line corresponds to $M_{K^*} = M_{K_1} = \infty$. The total number of events is also indicated in each case.

al. [15] (where $\simeq 700$ $\pi^+ \rightarrow e^+ \nu_e \gamma$ events had been observed). The theoretical branching ratio, calculated with the standard $V - A$ coupling, differs from the measured one by more than three standard deviations. This discrepancy may be avoided by adding to the standard matrix element the amplitude of a tensorial interaction [16]. Belyaev and Kogan [17] and Voloshin [18] have pointed out, however, that in the standard model the induced tensor coupling is too small to generate the rate observed in ref. [14].

Gabrielli [19] has worked out the effect of tensor couplings for $K^+ \rightarrow l^+ \nu_l \gamma$ decays. Using the above quoted values for the form factors A and V and a tensor coupling of a size suggested to explain the data in Ref. [14], he finds a $\leq 30\%$ effect in the partial decay rates (the exact size depends on the chosen coupling, channel, decay region,...). The author then suggests that these effects may be accessible to detection at high precision experiments carried out at DAΦNE.

We wish to point out that this may be difficult for the following reason. The calculation of the decays $K^+ \rightarrow l^+ \nu_l \gamma$ presented in this section is based on the one-loop formulae for the decay matrix elements. Higher-order effects may well be sizeable, see e.g. figure 1.3. There, it is explicitly seen that the effect of resonance exchange is $\simeq 30\%$ in particular regions of phase space. Therefore, in order to identify effects due to tensor couplings, one first has to pin down the contribution from higher-order effects in CHPT. This is not an easy task to achieve to the accuracy required. On the other hand, it is of course needless to say that the finding of a tensorial coupling of the size suggested in Ref. [16] would be

spectacular.

1.7 Improvements at DAΦNE

Previous experiments have used various cuts in phase space in order (i) to identify the individual contributions IB, SD^\pm , INT^\pm as far as possible, and (ii) to reduce the background from K_{l3} decays. This background has in fact forced so severe cuts that only the upper end of the lepton spectrum remained.

The experimental possibilities to reduce background from K_{l3} decays are presumably more favourable with today's techniques. Furthermore, the annual yield of $9 \cdot 10^9 K^+$ decays at DAΦNE is more than two orders of magnitude higher than the samples which were available in [4, 5, 7, 8]. This allows for a big improvement in the determination of the amplitudes A and V , in particular in $K_{\mu 2\gamma}$ decays. It would be very interesting to pin down the combination $L_9 + L_{10}$ of the low-energy constants which occur in the chiral representation of the amplitude A and to investigate the W^2 -dependence of the form factors.

2 The decays $K^\pm \rightarrow l^\pm \nu l'^+ l'^-$

Here we consider decays where the photon turns into a lepton-anti-lepton pair,

$$K^+ \rightarrow e^+ \nu \mu^+ \mu^- \quad (2.1)$$

$$K^+ \rightarrow \mu^+ \nu e^+ e^- \quad (2.2)$$

$$K^+ \rightarrow e^+ \nu e^+ e^- \quad (2.3)$$

$$K^+ \rightarrow \mu^+ \nu \mu^+ \mu^- . \quad (2.4)$$

2.1 Matrix elements

We start with the processes (2.1) and (2.2),

$$\begin{aligned} K^+(p) &\rightarrow l^+(p_l) \nu(p_\nu) l'^+(p_1) l'^-(p_2) \\ (l, l') &= (e, \mu) \text{ or } (\mu, e). \end{aligned} \quad (2.5)$$

The matrix element is

$$T = -i G_F e V_{us}^* \bar{\epsilon}_\rho \left\{ F_K \bar{L}^\rho - \bar{H}^{\rho\mu} l_\mu \right\} \quad (2.6)$$

where

$$\begin{aligned} \bar{L}^\mu &= m_l \bar{u}(p_\nu) (1 + \gamma_5) \left\{ \frac{2p^\mu - q^\mu}{2pq - q^2} - \frac{2p_l^\mu + \not{q} \gamma^\mu}{2p_l q + q^2} \right\} v(p_l) \\ l^\mu &= \bar{u}(p_\nu) \gamma^\mu (1 - \gamma_5) v(p_l) \end{aligned}$$

$$\begin{aligned}\overline{H}^{\rho\mu} = & iV_1\epsilon^{\rho\mu\alpha\beta}q_\alpha p_\beta - A_1(qWg^{\rho\mu} - W^\rho q^\mu) \\ & - A_2(q^2g^{\rho\mu} - q^\rho q^\mu) - A_4(qWq^\rho - q^2W^\rho)W^\mu\end{aligned}\quad (2.7)$$

with

$$A_4 = \frac{2F_K}{M_K^2 - W^2} \frac{F_V^K(q^2) - 1}{q^2} + A_3 . \quad (2.8)$$

The form factors $A_i(q^2, W^2)$, $V_1(q^2, W^2)$ are the ones defined in appendix C. $F_V^K(q^2)$ is the electromagnetic form factor of the K^+ . Finally the quantity $\overline{\epsilon}^\mu$ stands for

$$\overline{\epsilon}^\mu = \frac{e}{q^2} \overline{u}(p_2) \gamma^\mu v(p_1) , \quad (2.9)$$

and the four-momenta are

$$q = p_1 + p_2, \quad W = p_l + p_\nu = p - q \quad (2.10)$$

such that $q_\mu \overline{\epsilon}^\mu = 0$.

In order to obtain the matrix element for (2.3) and (2.4),

$$K^+(p) \rightarrow l^+(p_l) \nu(p_\nu) l^+(p_1) l^-(p_2) , \quad (2.11)$$

one identifies m_l and m_l' in (2.6) and subtracts the contribution obtained from interchanging $p_1 \leftrightarrow p_l$:

$$\begin{aligned}(p_1, p_l) & \rightarrow (p_l, p_1) \\ q & \rightarrow p_l + p_2 \\ W & \rightarrow p - q = p_\nu + p_1 .\end{aligned}\quad (2.12)$$

2.2 Decay distributions

The decay width is given by

$$d\Gamma = \frac{1}{2M_K(2\pi)^8} \sum_{spins} |T^2| d_{LIPS}(p; p_l, p_\nu, p_1, p_2) \quad (2.13)$$

and the total rate is the integral over this for the case $l \neq l'$. For the case $l = l'$ the integral has to be divided by the factor 2 for two identical particles in the final state.

We first consider the case where $l \neq l'$ and introduce the dimensionless variables

$$x = \frac{2pq}{M_K^2}, \quad y = \frac{2p_l p}{M_K^2}, \quad z = \frac{q^2}{M_K^2}, \quad r_l = \frac{m_l^2}{M_K^2}, \quad r_l' = \frac{m_{l'}^2}{M_K^2} . \quad (2.14)$$

Then one obtains, after integrating over p_1 and p_2 at fixed q^2 [20],

$$\begin{aligned}
d\Gamma_{K^+ \rightarrow l^+ \nu l'^+ l'^-} &= \alpha^2 G_F^2 |V_{us}|^2 M_K^5 F(z, r'_l) \left\{ - \sum_{spins} \overline{T}_\mu^* \overline{T}^\mu \right\} dx dy dz \\
F(z, r'_l) &= \frac{1}{192\pi^3 z} \left\{ 1 + \frac{2r'_l}{z} \right\} \sqrt{1 - \frac{4r'_l}{z}} \\
\overline{T}^\mu &= M_K^{-2} \left\{ F_K \overline{L}^\mu - \overline{H}^{\mu\nu} l_\nu \right\}.
\end{aligned} \tag{2.15}$$

This result allows one to evaluate, e.g., the distribution $d\Gamma/dz$ of produced $l'^+ l'^-$ pairs rather easily. The kinematically allowed region is

$$\begin{aligned}
4r'_l &\leq z \leq 1 + r_l - 2\sqrt{r_l} \\
2\sqrt{z} &\leq x \leq 1 + z - r_l \\
A - B &\leq y \leq A + B
\end{aligned} \tag{2.16}$$

with

$$\begin{aligned}
A &= \frac{(2-x)(1+z+r_l-x)}{2(1+z-x)} \\
B &= \frac{(1+z-x-r_l)\sqrt{x^2-4z}}{2(1+z-x)}.
\end{aligned} \tag{2.17}$$

The case $l = l'$ is slightly more elaborate. We feel that it does not make sense to display the term $\sum_{spins} |T|^2$ because it is of considerable complexity in the general case when all the form factors A_i , V_1 and F_V^K are q^2 and W^2 dependent. The expression together with the Monte Carlo program to do the phase space integrals is available on request from the authors.

2.3 Theory

The form factors A_i , V_1 and F_V^K have been discussed in all kinds of models, Vector Meson Dominance, hard meson, etc.. For a discussion see Ref. [9]. We will restrict ourselves to the predictions in the framework of CHPT.

To leading order we have

$$\begin{aligned}
V_1 &= 0 \\
A_1 &= A_2 = A_3 = 0.
\end{aligned} \tag{2.18}$$

We also have $F_V^K = 1$. The rate here is entirely given by the inner Bremsstrahlung contribution. At the one-loop level several form factors get non-zero values [11]

$$V_1 = -\frac{1}{8\pi^2 F}$$

Table 2.1: Theoretical values for the branching ratios for the decay $K^+ \rightarrow \mu^+ \nu e^+ e^-$ for various cuts.

	tree level	form factors as given by CHPT
full phase space	$2.49 \cdot 10^{-5}$	$2.49 \cdot 10^{-5}$
$z \leq 10^{-3}$	$2.07 \cdot 10^{-5}$	$2.07 \cdot 10^{-5}$
$z \geq 10^{-3}$	$4.12 \cdot 10^{-6}$	$4.20 \cdot 10^{-6}$
$z \geq (20 \text{ MeV}/M_K)^2$	$3.15 \cdot 10^{-6}$	$3.23 \cdot 10^{-6}$
$z \geq (140 \text{ MeV}/M_K)^2$	$4.98 \cdot 10^{-8}$	$8.51 \cdot 10^{-8}$
$x \geq 40 \text{ MeV}/M_K$	$1.58 \cdot 10^{-5}$	$1.58 \cdot 10^{-5}$

$$\begin{aligned}
A_1 &= -\frac{4}{F} (L_9^r + L_{10}^r) \\
A_2 &= -\frac{2F_K(F_V^K(q^2) - 1)}{q^2} \\
A_3 &= 0 \\
F_V^K(q^2) &= 1 + H_{\pi\pi}(q^2) + 2H_{KK}(q^2) .
\end{aligned} \tag{2.19}$$

These results obey the current algebra relation of Ref. [9]. The function $F_V^K(q^2)$ does, however, deviate somewhat from the linear parametrization often used. The function $H(t)$ is defined in appendix B.

The fact that the form factors at next-to-leading order could be written in terms of the kaon electromagnetic form factor in a simple way is not true anymore at the p^6 level. The Lagrangian at order p^6 contains a term of the form

$$\text{tr} \left\{ D_\alpha F_L^{\alpha\mu} U^\dagger D^\beta F_{R\beta\mu} U \right\} \tag{2.20}$$

that contributes to A_2 and A_3 but not to the kaon electromagnetic form factor, $F_V^K(q^2)$.

2.4 Numerical results

We have calculated the rates for a few cuts, including those given in the literature. For the case of unequal leptons, the results are given in table 2.1 for the decay $K^+ \rightarrow \mu^+ \nu e^+ e^-$. These include the cuts used in Refs. [20] and [21], $x \geq 40 \text{ MeV}/M_K$ and $z \geq (140 \text{ MeV}/M_K)^2$, respectively. It can be seen that for this decay most of the branching ratio is generated at very low electron-positron invariant masses. As can be seen from the result for the cuts used in Ref. [21], the effect of the structure dependent terms is most visible at high invariant electron-positron invariant mass. Our calculation, including the effect of the form factors agrees well with their data. We disagree, however, with the numerical result obtained by Ref. [20] by about an order of magnitude.

Table 2.2: Theoretical values for the branching ratios for the decay $K^+ \rightarrow e^+ \nu e^+ e^-$ for various cuts.

	tree level	form factors as given by CHPT
full phase space	$\approx 4 \cdot 10^{-9}$	$1.8 \cdot 10^{-7}$
$z, z_1 \geq 10^{-3}$	$3.0 \cdot 10^{-10}$	$1.22 \cdot 10^{-7}$
$z, z_1 \geq (50 \text{ MeV}/M_K)^2$	$5.2 \cdot 10^{-11}$	$8.88 \cdot 10^{-8}$
$z, z_1 \geq (140 \text{ MeV}/M_K)^2$	$2.1 \cdot 10^{-12}$	$3.39 \cdot 10^{-8}$

For the decay $K^+ \rightarrow e^+ \nu \mu^+ \mu^-$, we obtain for the tree level or IB contribution a branching ratio

$$BR_{IB}(K^+ \rightarrow e^+ \nu \mu^+ \mu^-) = 3.06 \cdot 10^{-12} \quad (2.21)$$

and, including the form factors,

$$BR_{total}(K^+ \rightarrow e^+ \nu \mu^+ \mu^-) = 1.12 \cdot 10^{-8}. \quad (2.22)$$

Here the structure dependent terms are the leading-contribution since the inner Bremsstrahlung contribution is helicity suppressed as can be seen from the factor m_l in \overline{L}_μ .

For the decays with identical leptons we obtain for the muon case a branching ratio of

$$BR_{total}(K^+ \rightarrow \mu^+ \nu \mu^+ \mu^-) = 1.35 \cdot 10^{-8} \quad (2.23)$$

for the full phase space including the effects of the form factors. The inner Bremsstrahlung or the tree level branching ratio for this decay is

$$BR_{IB}(K^+ \rightarrow \mu^+ \nu \mu^+ \mu^-) = 3.79 \cdot 10^{-9}. \quad (2.24)$$

For the decay with two positrons and one electron the integration over full phase space for the tree level results is very sensitive to the behaviour for small pair masses. We have given the tree level and the full prediction, including form factor effects in table 2.2. The cuts are always on both invariant masses :

$$\begin{aligned} z &= (p_1 + p_2)^2 / M_K^2 \\ z_1 &= (p_l + p_2)^2 / M_K^2 . \end{aligned} \quad (2.25)$$

The values for the masses used are those of K^+ and π^+ . For L_9 and L_{10} we used the values given in table 1 in Ref. [2],

$$\begin{aligned} L_9^r(M_\rho) &= 6.9 \cdot 10^{-3} \\ L_{10}^r(M_\rho) &= -5.5 \cdot 10^{-3} . \end{aligned} \quad (2.26)$$

2.5 Present experimental status

Only decays with an electron positron pair in the final state, decays (2.2) and (2.3), have been observed.

Both have been measured in the same experiment [21]. The decay $K^+ \rightarrow \mu^+ \nu e^+ e^-$ was measured with a branching ratio of $(1.23 \pm 0.32) \cdot 10^{-7}$ with a lower cut on the electron positron invariant mass of 140 MeV . The measurement is compatible with our calculation including the form factor effects for the relevant region of phase space. This measurement was then extrapolated [21] using the result of [20] to the full phase space. Since we disagree with that calculation, we also disagree with the extrapolation.

In the same experiment, 4 events of the type $K^+ \rightarrow e^+ \nu e^+ e^-$ were observed where both electron positron pair invariant masses were above 140 MeV . This corresponds to a branching ratio for this region of phase space of $(2.8_{-1.4}^{+2.8}) \cdot 10^{-8}$. This result is compatible within errors with our calculation, see table 2.2. The matrix element of Ref. [20] was again used for the extrapolation to full phase space [21]. Apart from our numerical disagreement, the calculation of Ref. [20] was for the case of non-identical leptons and cannot be applied here.

For the decay $K^+ \rightarrow \mu^+ \nu \mu^+ \mu^-$ an upper limit of $4.1 \cdot 10^{-7}$ exists [22]. This upper limit is compatible with our theoretical result, Eq. (2.23).

The decay $K^+ \rightarrow e^+ \nu \mu^+ \mu^-$ has not been looked for so far and should be within the capabilities of DAΦNE given the branching ratio predicted in the previous subsection. This decay proceeds almost entirely through the structure dependent terms and is as such a good test of our calculation.

2.6 Improvements at DAΦNE

The decays discussed in this subsection, $K^+ \rightarrow l^+ \nu l^+ l^-$, are complementary to the decays $K^+ \rightarrow l^+ \nu \gamma$. As was the case for the analogous decay, $\pi^+ \rightarrow e^+ \nu e^+ e^-$ [23], it may be possible to explore phase space more easily with this process than with $K^+ \rightarrow l^+ \nu \gamma$ to resolve ambiguities in the form factors.

As can be seen from our predictions, tables 2.1 and 2.2, all the decays considered in this subsection should be observable at DAΦNE. Large improvements in statistics are possible since less severe cuts than those used in the past experiments should be possible. In the decays with a $\mu^+ \mu^-$ pair and the decay $K^+ \rightarrow e^+ \nu e^+ e^-$ the effects of the form factors are already large in the total rates and should be easily visible at DAΦNE. In the decay $K^+ \rightarrow \mu^+ \nu e^+ e^-$ most of the total rate is for small invariant mass of the pair and is given by the inner Bremsstrahlung contribution. There are, however, regions of phase space where the form factor effects are large and DAΦNE should have enough statistics to be able to study these regions.

3 K_{l3} decays

The decay channels considered in this subsection are

$$K^+(p) \rightarrow \pi^0(p')l^+(p_l)\nu_l(p_\nu) \quad [K_{l3}^+] \quad (3.1)$$

$$K^0(p) \rightarrow \pi^-(p')l^+(p_l)\nu_l(p_\nu) \quad [K_{l3}^0] \quad (3.2)$$

and their charge conjugate modes. The symbol l stands for μ or e . We do not consider electromagnetic corrections and correspondingly set $\alpha = 0$ throughout this subsection.

3.1 Matrix elements and kinematics

The matrix element for K_{l3}^+ has the general structure

$$T = \frac{G_F}{\sqrt{2}} V_{us}^* l^\mu F_\mu^+(p', p) \quad (3.3)$$

with

$$\begin{aligned} l^\mu &= \bar{u}(p_\nu)\gamma^\mu(1 - \gamma_5)v(p_l) \\ F_\mu^+(p', p) &= \langle \pi^0(p') | V_\mu^{4-i5}(0) | K^+(p) \rangle \\ &= \frac{1}{\sqrt{2}} [(p' + p)_\mu f_+^{K^+\pi^0}(t) + (p - p')_\mu f_-^{K^+\pi^0}(t)]. \end{aligned} \quad (3.4)$$

To obtain the matrix element for K_{l3}^0 , one replaces F_μ^+ by

$$\begin{aligned} F_\mu^0(p', p) &= \langle \pi^-(p') | V_\mu^{4-i5}(0) | K^0(p) \rangle \\ &= (p' + p)_\mu f_+^{K^0\pi^-}(t) + (p - p')_\mu f_-^{K^0\pi^-}(t). \end{aligned} \quad (3.5)$$

The processes (3.1) and (3.2) thus involve the four K_{l3} form factors $f_\pm^{K^+\pi^0}(t)$, $f_\pm^{K^0\pi^-}(t)$ which depend on

$$t = (p' - p)^2 = (p_l + p_\nu)^2, \quad (3.6)$$

the square of the four momentum transfer to the leptons.

Let $f_\pm^{K\pi} = f_\pm^{K^+\pi^0}$ or $f_\pm^{K^0\pi^-}$. $f_+^{K\pi}$ is referred to as the vector form factor, because it specifies the P -wave projection of the crossed channel matrix elements $\langle 0 | V_\mu^{4-i5}(0) | K^+, \pi^0 \rangle$. The S -wave projection is described by the scalar form factor

$$f_0^{K\pi}(t) = f_+^{K\pi}(t) + \frac{t}{M_K^2 - M_\pi^2} f_-^{K\pi}(t). \quad (3.7)$$

Analyses of K_{l3} data frequently assume a linear dependence

$$f_{+,0}^{K\pi}(t) = f_+^{K\pi}(0) \left[1 + \lambda_{+,0} \frac{t}{M_{\pi^+}^2} \right]. \quad (3.8)$$

For a discussion of the validity of this approximation see [24, 3] and references cited therein. Eq. (3.8) leads to a constant $f_-^{K\pi}(t)$,

$$f_-^{K\pi}(t) = f_-^{K\pi}(0) = f_+^{K\pi}(0)(\lambda_0 - \lambda_+) \frac{M_K^2 - M_\pi^2}{M_{\pi+}^2}. \quad (3.9)$$

The form factors $f_{\pm,0}^{K\pi}(t)$ are analytic functions in the complex t -plane cut along the positive real axis. The cut starts at $t = (M_K + M_\pi)^2$. In our phase convention, the form factors are real in the physical region

$$m_l^2 \leq t \leq (M_K - M_\pi)^2. \quad (3.10)$$

The kinematics of (spin averaged) K_{l3} decays needs two variables, for which we choose

$$y = 2pp_l/M_K^2, \quad z = 2pp'/M_K^2 = (-t + M_\pi^2 + M_K^2)/M_K^2. \quad (3.11)$$

In the K rest frame, y (z) is proportional to the charged lepton (pion) energy,

$$y = 2E_l/M_K, \quad z = 2E_\pi/M_K. \quad (3.12)$$

The physical region for y and z is

$$\begin{aligned} 2\sqrt{r_l} &\leq y \leq 1 + r_l - r_\pi \\ A(y) - B(y) &\leq z \leq A(y) + B(y) \\ A(y) &= (2 - y)(1 + r_l + r_\pi - y)/[2(1 + r_l - y)] \\ B(y) &= \sqrt{y^2 - 4r_l}(1 + r_l - r_\pi - y)/[2(1 + r_l - y)] \\ r_l &= m_l^2/M_K^2, r_\pi = M_\pi^2/M_K^2. \end{aligned} \quad (3.13)$$

or, equivalently,

$$\begin{aligned} 2\sqrt{r_\pi} &\leq z \leq 1 + r_\pi - r_l \\ C(z) - D(z) &\leq y \leq C(z) + D(z) \\ C(z) &= (2 - z)(1 + r_\pi + r_l - z)/[2(1 + r_\pi - z)] \\ D(z) &= \sqrt{z^2 - 4r_\pi}(1 + r_\pi - r_l - z)/[2(1 + r_\pi - z)]. \end{aligned} \quad (3.14)$$

3.2 Decay rates

The differential decay rate for K_{l3}^+ is given by

$$d\Gamma = \frac{1}{2M_K(2\pi)^5} \sum_{spin.s} |T|^2 d_{LIPS}(p; p_l, p_\nu, p') \quad (3.15)$$

The Dalitz plot density

$$\rho(y, z) = \frac{d^2\Gamma}{dydz} = \frac{M_K}{256\pi^3} \sum_{spins} |T|^2 \quad (3.16)$$

is a Lorentz invariant function which contains $f_{\pm}^{K^+\pi^0}$ in the following form,

$$\rho(y, z) = \frac{M_K^5 G_F^2 |V_{us}|^2}{256\pi^3} \left[A(f_+^{K^+\pi^0})^2 + B f_+^{K^+\pi^0} f_-^{K^+\pi^0} + C(f_-^{K^+\pi^0})^2 \right] \quad (3.17)$$

with

$$\begin{aligned} A(y, z) &= 4(z + y - 1)(1 - y) + r_l[4y + 3z - 3] - 4r_\pi + r_l(r_\pi - r_l) \\ B(y, z) &= 2r_l(3 - 2y - z + r_l - r_\pi) \\ C(y, z) &= r_l(1 + r_\pi - z - r_l). \end{aligned} \quad (3.18)$$

The quantities (A, B, C) are related to the ones quoted by the PDG [3] by

$$(A, B, C) = \frac{8}{M_K^3} (A, B, C)_{\text{PDG}}. \quad (3.19)$$

To obtain the rate for K_{l3}^0 , one replaces in (3.17) $f_{\pm}^{K^+\pi^0}$ by $\sqrt{2}f_{\pm}^{K^0\pi^-}$.

For convenience we also display the $K_{\mu 3}/K_{e 3}$ rates evaluated in the approximation (3.8) for the form factors,

$$\begin{aligned} \Gamma(K_{\mu 3}^+)/\Gamma(K_{e 3}^+) &= \frac{0.645 + 2.087\lambda_+ + 1.464\lambda_0 + 3.375\lambda_+^2 + 2.573\lambda_0^2}{1 + 3.457\lambda_+ + 4.783\lambda_+^2} \\ \Gamma(K_{\mu 3}^0)/\Gamma(K_{e 3}^0) &= \frac{0.645 + 2.086\lambda_+ + 1.459\lambda_0 + 3.369\lambda_+^2 + 2.560\lambda_0^2}{1 + 3.456\lambda_+ + 4.776\lambda_+^2}. \end{aligned} \quad (3.20)$$

We have used the physical masses [3] in evaluating these ratios and M_{π^+} to scale the slope in both cases. The terms linear and quadratic in λ_0 are proportional to m_l^2 and therefore strongly suppressed in the electron case. We do not include them in the denominators, because these coefficients are smaller than 10^{-4} . The interference term $\lambda_0\lambda_+$ is absent by angular momentum conservation. Furthermore, one has

$$\int dy dz A(y, z) = \begin{cases} 0.0623 & [K_{\mu 3}^+] \\ 0.0606 & [K_{\mu 3}^0] \end{cases}. \quad (3.21)$$

3.3 Determination of the K_{l3} form factors

Measurements of the Dalitz plot distribution (3.17) of $K_{\mu 3}$ data allow one in principle to pin down the form factors (up to a sign) in the range $m_\mu^2 \leq t \leq (M_K - M_\pi)^2$. Measuring the $K_{\mu 3}/K_{e 3}$ branching ratio and then using (3.20) gives a relationship between λ_+ and λ_0 which is valid in the approximation (3.8). Furthermore, muon polarization experiments

measure the weighted average of the ratio $f_-^{K\pi}(t)/f_+^{K\pi}(t)$ over the t range of the experiment [3, 25]. On the other hand, the electron modes K_{e3} are sensitive to $f_+^{K\pi}$ only, because the other contributions are suppressed by the factor $(m_e/M_K)^2 \simeq 10^{-6}$, see eqs. (3.17), (3.18).

Isospin breaking effects in $f_+^{K^+\pi^0}(0)$ and $f_+^{K^0\pi^-}(0)$ play a central role in the determination of the Kobayashi-Maskawa matrix element V_{us} from K_{e3} data, see [26] for a detailed discussion of this point. In the following we concentrate on the measurement of the slopes $\lambda_{+,0}$.

3.4 Previous measurements

We refer the reader to the 1982 version of the PDG [27]⁴ for a critical discussion of the wealth of experimental information on $\lambda_{+,0}^{K\pi}$. Here we content ourselves with a short summary.

K_{e3} -experiments

The λ_+ values obtained are fairly consistent. The average values are

$$\begin{aligned} K_{e3}^+ : \lambda_+ &= 0.028 \pm 0.004 \quad \text{Ref. [3]} \\ K_{e3}^0 : \lambda_+ &= 0.030 \pm 0.0016 \quad \text{Ref. [3]} . \end{aligned} \quad (3.22)$$

$K_{\mu 3}$ -experiments

The result by Donaldson et al. [28]

$$\begin{aligned} \lambda_+ &= 0.030 \pm 0.003 \\ \lambda_0 &= 0.019 \pm 0.004 \end{aligned} \quad (3.23)$$

dominates the statistics in the $K_{\mu 3}^0$ case. The λ_+ value (3.23) is consistent with the K_{e3} value (3.22). However, the situation concerning the slope λ_0 is rather unsatisfactory, as the following (chronological) list illustrates.

$$\lambda_0 = \left\{ \begin{array}{lll} 0.0341 & \pm & 0.0067 \quad [29] \\ 0.050 & \pm & 0.008 \quad [30] \\ 0.039 & \pm & 0.010 \quad [31] \\ 0.047 & \pm & 0.009 \quad [32] \\ 0.025 & \pm & 0.019 \quad [33] \\ 0.019 & \pm & 0.004 \quad [28] . \end{array} \right. \quad (3.24)$$

The χ^2 fit to the $K_{\mu 3}^0$ data yields $\lambda_+ = 0.034 \pm 0.005$, $\lambda_0 = 0.025 \pm 0.006$ with a $\chi^2/DF = 88/16$ [27, p.76]! The situation in the charged mode $K_{\mu 3}^+$ is slightly better [27].

⁴Please note that the most recent measurements of $\lambda_{+,0}$ go back to 1981 [3]!

3.5 Theory

The theoretical prediction of K_{l3} form factors has a long history, starting in the sixties with the current algebra evaluation of $f_{\pm}^{K^+\pi^0}$. For an early review of the subject and for references to work prior to CHPT evaluations of f_{\pm} we refer the reader to [34] (see also Ref.[35]). Here we concentrate on the evaluation of the form factors in the framework of CHPT. We restrict our consideration to the isospin symmetry limit $m_u = m_d$, as a result of which one has

$$f_{\pm,0}^{K^0\pi^-}(t) = f_{\pm,0}^{K^+\pi^0}(t) \equiv f_{\pm,0}(t) ; m_u = m_d . \quad (3.25)$$

3.5.1 Chiral prediction at one-loop order

In Ref. [24], the vector current matrix elements $\langle M' | q\gamma^\mu \frac{\lambda^a}{2} q | M \rangle$ have been calculated up to and including terms of order $t = (p' - p)^2$ and of order m_u, m_d and m_s in the invariant form factors. For reasons which will become evident below, we consider here, in addition to the K_{l3} form factors, also the electromagnetic form factor of the pion

$$\langle \pi^+(p') | V_{em}^\mu(0) | \pi^+(p) \rangle = (p' + p)^\mu F_V^\pi(t). \quad (3.26)$$

The low-energy representation for $F_V^\pi(t)$ [24, 36] and $f_+(t)$ [24] reads

$$\begin{aligned} F_V^\pi(t) &= 1 + 2H_{\pi\pi}(t) + H_{KK}(t) \\ f_+(t) &= 1 + \frac{3}{2}H_{K\pi}(t) + \frac{3}{2}H_{K\eta}(t). \end{aligned} \quad (3.27)$$

The quantity $H(t)$ is a loop function displayed in appendix B. It contains the low-energy constant L_9 . The indices attached to $H(t)$ denote the masses running in the loop.

Since L_9 is the only unknown occurring in $F_V^\pi(t)$ and in $f_+(t)$, we need experimental information on the *slope* of one of these two form factors to obtain a parameter-free low-energy representation of the other.

The analogous low-energy representation of the scalar form factor is

$$\begin{aligned} f_0(t) &= 1 + \frac{1}{8F^2} \left(5t - 2\Sigma_{K\pi} - 3\frac{\Delta_{K\pi}^2}{t} \right) \bar{J}_{K\pi}(t) \\ &+ \frac{1}{24F^2} \left(3t - 2\Sigma_{K\pi} - \frac{\Delta_{K\pi}^2}{t} \right) \bar{J}_{K\eta}(t) \\ &+ \frac{t}{\Delta_{K\pi}} \left(\frac{F_K}{F_\pi} - 1 \right). \end{aligned} \quad (3.28)$$

The function $\bar{J}(t)$ is listed in appendix B, and $\Sigma_{K\pi}$ and $\Delta_{K\pi}$ stand for

$$\begin{aligned} \Sigma_{K\pi} &= M_K^2 + M_\pi^2 \\ \Delta_{K\pi} &= M_K^2 - M_\pi^2 . \end{aligned} \quad (3.29)$$

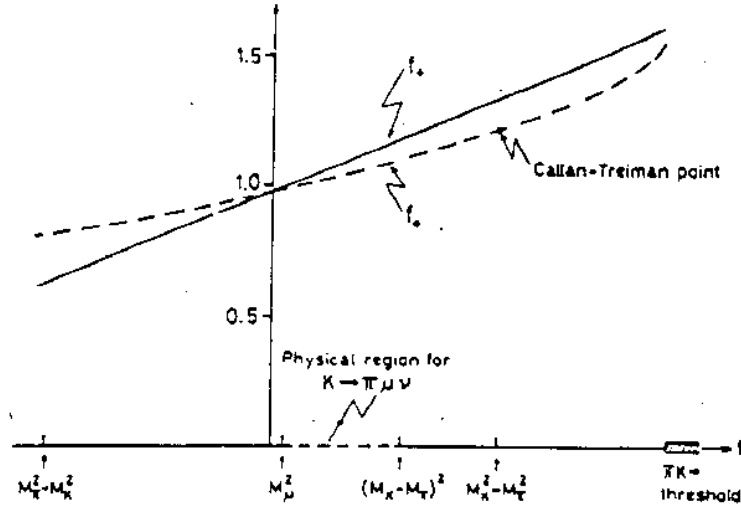


Figure 3.1: The vector and scalar form factors $f_+(t)$ and $f_0(t)$.

The measured value [26] $F_K/F_\pi = 1.22 \pm 0.01$ may be used to obtain a parameter-free prediction of the scalar form factor $f_0(t)$.

3.5.2 Momentum dependence of the vector form factor

In the spacelike interval $\sqrt{-t} < 350$ MeV the low-energy representation (3.27) for the electromagnetic form factor $F_V^\pi(t)$ is very well approximated by the first two terms in the Taylor series expansion around $t = 0$,

$$F_V^\pi(t) = 1 + \frac{1}{6} \langle r^2 \rangle_V^\pi t + \dots \quad (3.30)$$

Likewise, the linear approximation

$$f_+(t) = f_+(0) \left\{ 1 + \frac{1}{6} \langle r^2 \rangle_V^{K\pi} t + \dots \right\} \quad (3.31)$$

reproduces the low-energy representation (3.27) very well, see Fig. 3.1. This is in agreement with the observed Dalitz plot distribution, which is consistent with a form factor linear in t . The charge radii are

$$\langle r^2 \rangle_V^\pi = \frac{12L_9^r}{F^2} - \frac{1}{32\pi^2 F^2} \left\{ 2 \ln \frac{M_\pi^2}{\mu^2} + \ln \frac{M_K^2}{\mu^2} + 3 \right\}$$

$$\begin{aligned}
\langle r^2 \rangle_V^{K\pi} = \langle r^2 \rangle_V^\pi &- \frac{1}{64\pi^2 F^2} \left\{ 3h_1 \left(\frac{M_\pi^2}{M_K^2} \right) + 3h_1 \left(\frac{M_\eta^2}{M_K^2} \right) \right. \\
&\left. + \frac{5}{2} \ln \frac{M_K^2}{M_\pi^2} + \frac{3}{2} \ln \frac{M_\eta^2}{M_K^2} - 6 \right\}
\end{aligned} \tag{3.32}$$

where

$$h_1(x) = \frac{1}{2} \frac{(x^3 - 3x^2 - 3x + 1)}{(x-1)^3} \ln x + \frac{1}{2} \left(\frac{x+1}{x-1} \right)^2 - \frac{1}{3} . \tag{3.33}$$

To evaluate these relations numerically, we use the measured charge radius of the pion:

$$\langle r^2 \rangle_V^\pi = 0.439 \pm 0.008 \text{fm}^2 \quad [37] \tag{3.34}$$

as input and obtain the prediction

$$\lambda_+ = \frac{1}{6} M_{\pi^+}^2 \langle r^2 \rangle_V^{K\pi} = 0.031 \tag{3.35}$$

in agreement with the experimental results (3.22), (3.23) ⁵. From this (and from the considerably more detailed discussion in Ref. [24]), one concludes, in agreement with other theoretical investigations [38], that the measured charge radii $\langle r^2 \rangle_V^\pi$ and $\langle r^2 \rangle_V^{K\pi}$ are consistent with the low-energy prediction.

3.5.3 Momentum dependence of the scalar form factor. Dashen-Weinstein and Callan-Treiman relations

In the physical region of K_{l3} decay the low-energy representation (3.28) for the scalar form factor is approximated by the linear formula

$$f_0(t) = f_+(0) \left\{ 1 + \frac{1}{6} \langle r^2 \rangle_S^{K\pi} t + \dots \right\} \tag{3.36}$$

to within an accuracy of 1 %. (See Fig. 3.1). The curvature generated by higher-order terms is also expected to be negligible in the physical region of the decay [24]. For the slope $\langle r^2 \rangle_S^{K\pi}$ one obtains

$$\begin{aligned}
\langle r^2 \rangle_S^{K\pi} &= \frac{6}{M_K^2 - M_\pi^2} \left(\frac{F_K}{F_\pi} - 1 \right) + \delta_2 + O(\hat{m}, m_s) \\
\delta_2 &= -\frac{1}{192\pi^2 F^2} \left\{ 15h_2 \left(\frac{M_\pi^2}{M_K^2} \right) + \frac{19M_K^2 + 3M_\eta^2}{M_K^2 + M_\eta^2} h_2 \left(\frac{M_\eta^2}{M_K^2} \right) - 18 \right\}
\end{aligned} \tag{3.37}$$

⁵We do not quote an error for the result (3.35), because one should estimate higher-order chiral corrections for this purpose.

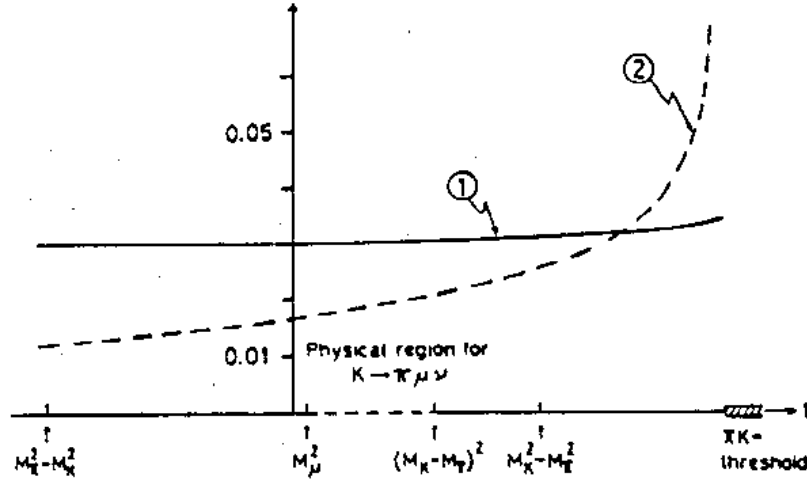


Figure 3.2: The normalized slopes of the vector and the scalar form factors. Curve 1: the normalized slope $M_{\pi+}^2 df_+(t)/dt$. Curve 2: the normalized slope $M_{\pi+}^2 df_0(t)/dt$. Near the πK threshold $t_0 = (M_K + M_\pi)^2$, the vector form factor behaves as $f_+(t) = f_+(t_0) + O[(t - t_0)]$, whereas $f_0(t) = f_0(t_0) + O[(\sqrt{t - t_0})]$. The slope of the scalar form factor is therefore singular at $t = (M_K + M_\pi)^2$.

where

$$\begin{aligned}
 h_2(x) &= \frac{3}{2} \left(\frac{1+x}{1-x} \right)^2 + \frac{3x(1+x)}{(1-x)^3} \ln x, \\
 h_2(x) &= h_2 \left(\frac{1}{x} \right), \quad h_2(1) = 1, \\
 \hat{m} &= (m_u + m_d)/2.
 \end{aligned} \tag{3.38}$$

This (parameter-free) prediction is a modified version of the Dashen-Weinstein relation [39], which results if the nonanalytic contribution δ_2 is dropped. Dashen, Li, Pagels and Weinstein [40] were the first to point out that the low-energy singularities generated by the Goldstone bosons affect this relation. The modified relation is formulated as a prediction for the slope of $f_0(t)$ at the unphysical point $t_1 = M_K^2 + M_\pi^2$. Their expression for this slope however has two shortcomings: (i) it does not account for all corrections of order \mathcal{M} ; (ii) The slope at t_1 differs substantially from the slope in the physical region of the decay [24, 41], see Fig. 3.2.

Algebraically, the correction δ_2 is of the same order in the low-energy expansion as the term involving $F_K/F_\pi - 1$. Numerically, the correction is however small: δ_2 reduces the

prediction by 11 %. With $F_K/F_\pi = 1.22 \pm 0.01$ the low-energy theorem (3.37) implies

$$\begin{aligned} \langle r^2 \rangle_S^{K\pi} &= 0.20 \pm 0.05 \text{fm}^2 \\ \lambda_0 &= \frac{1}{6} M_{\pi^+}^2 \langle r^2 \rangle_S^{K\pi} = 0.017 \pm 0.004 \end{aligned} \quad (3.39)$$

where the error is an estimate of the uncertainties due to higher-order contributions. The prediction (3.39) is in agreement with the high-statistics experiment [28] quoted in (3.23) but in flat disagreement with some of the more recent data listed in (3.24).

In the formulation of Dashen and Weinstein [39], the Callan-Treiman relation [42] states that the scalar form factor evaluated at $t = M_K^2 - M_\pi^2$ differs from F_K/F_π only by terms of order m_u, m_d : the quantity

$$\Delta_{\text{CT}} = f_0(M_K^2 - M_\pi^2) - \frac{F_K}{F_\pi} \quad (3.40)$$

is of order \hat{m} . Indeed, the low-energy representation (3.28) leads to

$$\Delta_{\text{CT}} = -\frac{M_\pi^2}{2F^2} \left\{ \bar{J}_{K\pi}(M_K^2 - M_\pi^2) + \frac{1}{3} \bar{J}_{K\eta}(M_K^2 - M_\pi^2) \right\} + O(\hat{m}m_s) \quad (3.41)$$

Numerically, $\Delta_{\text{CT}} = -3.5 \cdot 10^{-3}$. The Callan-Treiman relation should therefore hold to a very high degree of accuracy. If the form factor is linear from $t = 0$ to $t = M_K^2 - M_\pi^2$ then the slope must be very close to

$$\lambda_0^{\text{CT}} = \frac{M_{\pi^+}^2}{M_K^2 - M_\pi^2} \left(\frac{F_K}{F_\pi} - 1 \right) = 0.019, \quad (3.42)$$

in agreement with (3.39) and with the experimental result of Ref. [28], but in disagreement with, e.g., the value found in Ref. [30]. We see no way to reconcile the value $\lambda_0 = 0.050$ with chiral symmetry.

3.6 Comment on tensor couplings

S.A. Akimenko et al. [43] have investigated the general form of the matrix element for K_{e3} decays, obtained by adding scalar and tensor couplings to the standard $V - A$ interaction. Analyzing the Dalitz-plot distribution of $3.2 \cdot 10^4$ $K^+ \rightarrow \pi^0 e^+ \nu_e$ events, they find that the presence of scalar and tensor couplings or nonlinearities in the form factor f_+ cannot be excluded. DAΦNE may be an ideal place to check this claim ($\simeq 4 \cdot 10^8$ $K^+ \rightarrow \pi^0 e^+ \nu_e$ events in one year). However, the same proviso as in the case of radiative K_{l2} decays should be made (see subsection 1.6): before any firm conclusion can be drawn, one has to estimate the effect of higher-order terms in the chiral calculation. In the present case this may be less difficult to achieve than in radiative kaon decays, as only one form factor comes into play, which, in addition, depends on one kinematical variable only.

Table 3.1: Rates of K_{l3} decays. The number of events in the third column corresponds to those data which are of relevance for the determination of the slope λ_0 of the scalar form factor.

		# events		
	branching ratio	Particle Data Group	DAΦNE 1 year	improvement
$K^+ \rightarrow \pi^0 \mu^+ \nu_\mu$	$3.18 \cdot 10^{-2}$	10^5	$3 \cdot 10^8$	$3 \cdot 10^3$
$K_L \rightarrow \pi^\pm \mu^\mp \nu$	$27 \cdot 10^{-2}$	$4 \cdot 10^6$	$3 \cdot 10^8$	70

3.7 Improvements at DAΦNE

DAΦNE provides the opportunity to improve our knowledge of K_{l3} decays in a very substantial manner - in particular, it should be possible to clarify the issue of the slope λ_0 of the scalar form factor f_0 . To illustrate, we compare in table 3.1 the hitherto obtained number of events (third column) with the expected ones at DAΦNE (fourth column). The last column displays the remarkable increase in statistics obtainable at DAΦNE.

4 Radiative K_{l3} decays

The decay channels considered in this subsection are

$$\begin{aligned} K^+(p) &\rightarrow \pi^0(p') l^+(p_l) \nu_l(p_\nu) \gamma(q) & [K_{l3\gamma}^+] \\ K^0(p) &\rightarrow \pi^-(p') l^+(p_l) \nu_l(p_\nu) \gamma(q) & [K_{l3\gamma}^0] \end{aligned}$$

and the charge conjugate modes. We only consider real photons ($q^2 = 0$).

4.1 Matrix elements

The matrix element for $K_{l3\gamma}^+$ has the general structure

$$\begin{aligned} T = & \frac{G_F}{\sqrt{2}} e V_{us}^* \varepsilon^\mu(q)^* \left\{ (V_{\mu\nu}^+ - A_{\mu\nu}^+) \bar{u}(p_\nu) \gamma^\nu (1 - \gamma_5) v(p_l) \right. \\ & \left. + \frac{F_\nu^+}{2 p_l q} \bar{u}(p_\nu) \gamma^\nu (1 - \gamma_5) (m_l - \not{p}_l - \not{q}) \gamma_\mu v(p_l) \right\} \equiv \varepsilon^{\mu*} A_\mu^+. \end{aligned} \quad (4.1)$$

The diagram of Fig. 4.1.a corresponding to the first part of Eq. (4.1) includes Bremsstrahlung off the K^+ . The lepton Bremsstrahlung diagram of Fig. 4.1.b is represented by the

second part of Eq. (4.1). The hadronic tensors $V_{\mu\nu}^+, A_{\mu\nu}^+$ are defined as

$$I_{\mu\nu}^+ = i \int d^4x e^{iqx} \langle \pi^0(p') | T \{ V_{\mu}^{em}(x) I_{\nu}^{4-i5}(0) \} | K^+(p) \rangle, \quad I = V, A. \quad (4.2)$$

F_{ν}^+ is the K_{l3}^+ matrix element

$$F_{\nu}^+ = \langle \pi^0(p') | V_{\nu}^{4-i5}(0) | K^+(p) \rangle. \quad (4.3)$$

The tensors $V_{\mu\nu}^+$ and $A_{\mu\nu}^+$ satisfy the Ward identities

$$\begin{aligned} q^{\mu} V_{\mu\nu}^+ &= F_{\nu}^+ \\ q^{\mu} A_{\mu\nu}^+ &= 0 \end{aligned} \quad (4.4)$$

leading in turn to

$$q^{\mu} A_{\mu}^+ = 0, \quad (4.5)$$

as is required by gauge invariance.

For $K_{l3\gamma}^0$, one obtains the corresponding amplitudes and hadronic tensors by making the replacements

$$\begin{aligned} K^+ &\rightarrow K^0, & \pi^0 &\rightarrow \pi^- \\ V_{\mu\nu}^+ &\rightarrow V_{\mu\nu}^0, & A_{\mu\nu}^+ &\rightarrow A_{\mu\nu}^0 \\ F_{\nu}^+ &\rightarrow F_{\nu}^0, & A_{\mu}^+ &\rightarrow A_{\mu}^0. \end{aligned} \quad (4.6)$$

To make the infrared behaviour transparent, it is convenient to separate the tensors $V_{\mu\nu}^+, V_{\mu\nu}^0$ into two parts:

$$\begin{aligned} V_{\mu\nu}^+ &= \hat{V}_{\mu\nu}^+ + \frac{p_{\mu}}{pq} F_{\nu}^+ \\ V_{\mu\nu}^0 &= \hat{V}_{\mu\nu}^0 + \frac{p'_{\mu}}{p'q} F_{\nu}^0. \end{aligned} \quad (4.7)$$

Due to Low's theorem, the amplitudes $\hat{V}_{\mu\nu}^{+,0}$ are finite for $q \rightarrow 0$. The axial amplitudes $A_{\mu\nu}^{+,0}$ are automatically infrared finite. The Ward identity (4.4) implies that the vector amplitudes $\hat{V}_{\mu\nu}^{+,0}$ are transverse:

$$q^{\mu} \hat{V}_{\mu\nu}^{+,0} = 0. \quad (4.8)$$

For on-shell photons, Lorentz and parity invariance together with gauge invariance allow the general decomposition (dropping the superscripts $+,0$ and terms that vanish upon contraction with the photon polarization vector)

$$\begin{aligned} \hat{V}_{\mu\nu} &= V_1 \left(g_{\mu\nu} - \frac{W_{\mu} q_{\nu}}{qW} \right) + V_2 \left(p'_{\mu} q_{\nu} - \frac{p'q}{qW} W_{\mu} q_{\nu} \right) \\ &\quad + V_3 \left(p'_{\mu} W_{\nu} - \frac{p'q}{qW} W_{\mu} W_{\nu} \right) + V_4 \left(p'_{\mu} p'_{\nu} - \frac{p'q}{qW} W_{\mu} p'_{\nu} \right) \\ A_{\mu\nu} &= i \varepsilon_{\mu\nu\rho\sigma} (A_1 p'^{\rho} q^{\sigma} + A_2 q^{\rho} W^{\sigma}) + i \varepsilon_{\mu\lambda\rho\sigma} p'^{\lambda} q^{\rho} W^{\sigma} (A_3 W_{\nu} + A_4 p'_{\nu}) \\ F_{\nu} &= C_1 p'_{\nu} + C_2 (p - p')_{\nu} \\ W &= p_l + p_{\nu}. \end{aligned} \quad (4.9)$$

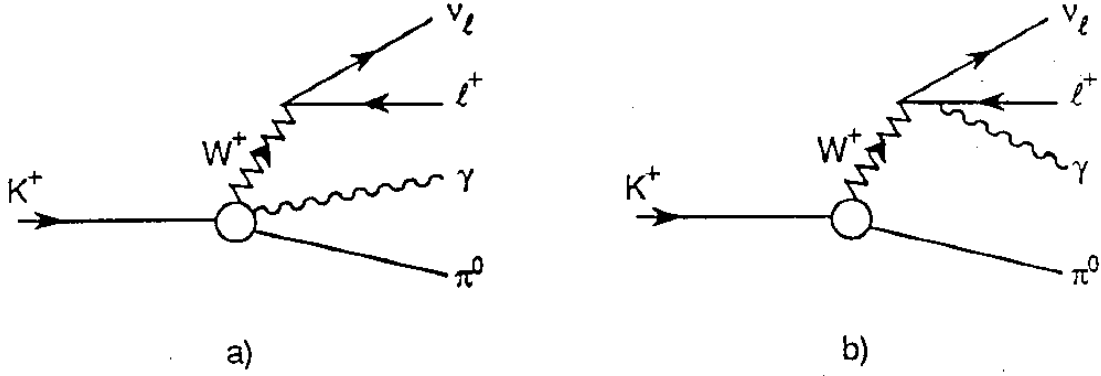


Figure 4.1: Diagrammatic representation of the $K_{l3\gamma}^+$ amplitude.

With the decomposition (4.7) we can write the matrix element for $K_{l3\gamma}^+$ in (4.1) in a form analogous to Eq. (1.2) for $K_{l2\gamma}$:

$$T = \frac{G_F}{\sqrt{2}} e V_{us}^* \varepsilon^\mu(q)^* \left\{ (\hat{V}_{\mu\nu}^+ - A_{\mu\nu}^+) \bar{u}(p_\nu) \gamma^\nu (1 - \gamma_5) v(p_l) + F_\nu^+ \bar{u}(p_\nu) \gamma^\nu (1 - \gamma_5) \left[\frac{p_\mu}{pq} - \frac{(\not{p}_l + \not{q} - m_l) \gamma_\mu}{2p_l q} \right] v(p_l) \right\}. \quad (4.10)$$

The four invariant vector amplitudes V_1, \dots, V_4 and the four axial amplitudes A_1, \dots, A_4 are functions of three scalar variables. A convenient choice for these variables is

$$E_\gamma = pq/M_K, \quad E_\pi = pp'/M_K, \quad W = \sqrt{W^2} \quad (4.11)$$

where W is the invariant mass of the lepton pair. The amplitudes C_1, C_2 can be expressed in terms of the K_{l3} form factors and depend only on the variable $(p-p')^2 = M_K^2 + M_\pi^2 - 2M_K E_\pi$. For the full kinematics of $K_{l3\gamma}$ two more variables are needed, e.g.

$$E_l = pp_l/M_K, \quad x = p_l q/M_K^2. \quad (4.12)$$

The variable x is related to the angle $\theta_{l\gamma}$ between the photon and the charged lepton in the K rest frame:

$$x M_K^2 = E_\gamma (E_l - \sqrt{E_l^2 - m_l^2} \cos \theta_{l\gamma}). \quad (4.13)$$

T invariance implies that the vector amplitudes V_1, \dots, V_4 , the axial amplitudes A_1, \dots, A_4 and the K_{l3} form factors C_1, C_2 are (separately) relatively real in the physical region. We choose the standard phase convention in which all amplitudes are real.

For $\theta_{l\gamma} \rightarrow 0$ (collinear lepton and photon), there is a lepton mass singularity in (4.1) which is numerically relevant for $l = e$. The region of small $E_\gamma, \theta_{l\gamma}$ is dominated by the K_{l3} matrix elements. The new theoretical information of $K_{l3\gamma}$ decays resides in the tensor amplitudes $\hat{V}_{\mu\nu}$ and $A_{\mu\nu}$. The relative importance of these contributions can be enhanced by cutting away the region of low $E_\gamma, \theta_{l\gamma}$. It may turn out to be of advantage to reduce the statistics by applying more severe cuts than necessary from a purely experimental point of view.

4.2 Decay rates

The total decay rate is given by

$$\Gamma(K \rightarrow \pi l \nu \gamma) = \frac{1}{2M_K(2\pi)^8} \int d_{LIPS}(p; p', p_l, p_\nu, q) \sum_{spins} |T|^2 \quad (4.14)$$

in terms of the amplitude T in (4.1). The square of the matrix element, summed over photon and lepton polarizations, is a bilinear form in the invariant amplitudes $V_1, \dots, V_4, A_1, \dots, A_4, C_1, C_2$. Pulling out common factors, we write (4.14) in the form

$$\Gamma(K \rightarrow \pi l \nu \gamma) = \frac{4\alpha G_F^2 |V_{us}|^2}{(2\pi)^7 M_K} \int d_{LIPS}(p; p', p_l, p_\nu, q) SM \quad (4.15)$$

where SM is the reduced matrix element. For the actual numerical calculations, we have found it useful to employ a tensor decomposition different from the one in Eqs. (4.7) and (4.9)

$$\begin{aligned} V_{\mu\nu} = & B_1 g_{\mu\nu} + B_2 W_\mu q_\nu + B_3 p'_\mu q_\nu + B_4 W_\mu p'_\nu \\ & + B_5 W_\mu W_\nu + B_6 p'_\mu W_\nu + B_7 p'_\mu p'_\nu \end{aligned} \quad (4.16)$$

One advantage is that (4.16) applies equally well to both charge modes while (4.7) does not. In the numerical evaluation of the amplitudes, gauge invariance can of course be used to express three of the B_i in terms of the remaining ones and of C_1, C_2 .

To get some feeling for the magnitude of the various decay rates, let us first consider the tree level amplitudes to lowest order p^2 in CHPT. With the sign conventions of Ref. [44], these amplitudes are [11, 45] :

$K_{l3\gamma}^+$:

$$\begin{aligned} V_{\mu\nu}^+ &= \frac{1}{\sqrt{2}} \left[g_{\mu\nu} + \frac{(p' + W)_\mu (2p' + W)_\nu}{pq} \right] \\ A_{\mu\nu}^+ &= 0 \\ F_\nu^+ &= \frac{1}{\sqrt{2}} (p + p')_\nu \end{aligned} \quad (4.17)$$

Table 4.1: Branching ratios for tree level amplitudes for $E_\gamma \geq 30 MeV$ and $\theta_{l\gamma} \geq 20^\circ$ in the K rest frame.

decay	BR(tree)	#events/yr
$K_{e3\gamma}^+$	2.8×10^{-4}	2.5×10^6
$K_{\mu3\gamma}^+$	1.9×10^{-5}	1.7×10^5
$K_{e3\gamma}^0$	3.6×10^{-3}	4.0×10^6
$K_{\mu3\gamma}^0$	5.2×10^{-4}	5.7×10^5

Table 4.2: Experimental results for $K_{l3\gamma}$ decays

decay	exp.	$E_{\gamma,min}$	# events	BR	
$K_{e3\gamma}^+$	[46]	$10 MeV$	192	$(2.7 \pm 0.2) \times 10^{-4}$	$0.6 < \cos \theta_{e\gamma} < 0.9$
$K_{e3\gamma}^+$	[47]	$10 MeV$	13	$(3.7 \pm 1.3) \times 10^{-4}$	—” —
$K_{e3\gamma}^+$	[48]	$30 MeV$	16	$(2.3 \pm 1.0) \times 10^{-4}$	$\cos \theta_{e\gamma} < 0.9$
$K_{\mu3\gamma}^+$	[48]	$30 MeV$	0	$< 6.1 \times 10^{-5}$	90% <i>c.l.</i>
$K_{e3\gamma}^0$	[49]	$15 MeV$	10	$(1.3 \pm 0.8) \times 10^{-2}$	

$K_{l3\gamma}^0$:

$$\begin{aligned}
V_{\mu\nu}^0 &= -g_{\mu\nu} + \frac{p'_\mu(2p' + 2q + W)_\nu}{p'q} \\
A_{\mu\nu}^0 &= 0 \\
F_\nu^0 &= (p + p')_\nu.
\end{aligned} \tag{4.18}$$

In table 4.1 the corresponding branching ratios are presented for the four decay modes for $E_\gamma \geq 30 MeV$ and $\theta_{l\gamma} \geq 20^\circ$. For $K_{l3\gamma}^0$, the rates are to be understood as $\Gamma(K_L \rightarrow \pi^\pm l^\mp \nu \gamma)$. The number of events correspond to the design values for DAΦNE (cf. App. A).

4.3 Previous experiments

The data sample for $K_{l3\gamma}$ decays is very limited and it is obvious that DAΦNE will be able to make significant improvements. The present experimental status is summarized in table 4.2.

A comparison between tables 4.1 and 4.2 shows the tremendous improvement in statistics to be expected at DAΦNE. We shall come back to the question whether this improve-

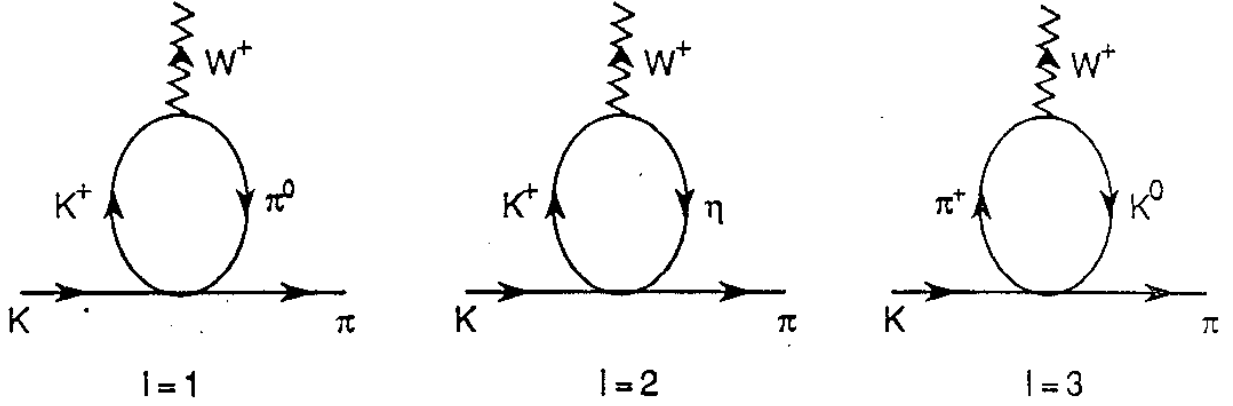


Figure 4.2: Loop diagrams (without tadpoles) for K_{l3} at $O(p^4)$. For $K_{l3\gamma}$, the photon must be appended on all charged lines and on all vertices.

ment will be sufficient to test the standard model at the next-to-leading order, $O(p^4)$, in CHPT.

4.4 Theory

Prior to CHPT, the most detailed calculations of $K_{l3\gamma}$ amplitudes were performed by Fearing, Fischbach and Smith [50] using current algebra techniques.

In the framework of CHPT, the amplitudes are given by (4.17) and (4.18) to leading order in the chiral expansion.

4.4.1 CHPT to $O(p^4)$ [11]

There are in general three types of contributions [44]: anomaly, local contributions due to \mathcal{L}_4 and loop amplitudes.

The anomaly contributes to the axial amplitudes

$$\begin{aligned} A_{\mu\nu}^+ &= \frac{i\sqrt{2}}{16\pi^2 F^2} \left\{ \varepsilon_{\mu\nu\rho\sigma} q^\rho (4p' + W)^\sigma + \frac{4}{W^2 - M_K^2} \varepsilon_{\mu\lambda\rho\sigma} W_\nu p'^\lambda q^\rho W^\sigma \right\} \\ A_{\mu\nu}^0 &= -\frac{i}{8\pi^2 F^2} \varepsilon_{\mu\nu\rho\sigma} q^\rho W^\sigma. \end{aligned} \quad (4.19)$$

The loop diagrams for $K_{l3\gamma}$ are shown in Fig. 4.2. We first write the K_{l3}^+ matrix element in terms of three functions f_1^+, f_2^+, f_3^+ which will also appear in the invariant amplitudes

Table 4.3: Coefficients for the $K_{l3\gamma}^+$ loop amplitudes corresponding to the diagrams $I = 1, 2, 3$ in Fig. 4.2. All coefficients c_i^I must be divided by $6\sqrt{2}F^2$.

I	M_I	m_I	c_1^I	c_2^I	c_3^I
1	M_K	M_π	1	-2	$-M_K^2 - 2M_\pi^2$
2	M_K	M_η	3	-6	$-M_K^2 - 2M_\pi^2$
3	M_π	M_K	0	-6	$-6M_\pi^2$

V_i^+ . Including the contributions from the low-energy constants L_5, L_9 in \mathcal{L}_4 , the K_{l3} matrix element F_ν^+ is given by

$$\begin{aligned}
F_\nu^+ &= f_1^+(t)p'_\nu + \left[\frac{1}{2}(M_K^2 - M_\pi^2 - t)f_2^+(t) + f_3^+(t) \right] (p - p')_\nu \\
f_1^+(t) &= \sqrt{2} + \frac{4\overline{L}_9}{\sqrt{2}F^2}t + 2 \sum_{I=1}^3 (c_2^I - c_1^I) B_2^I(t) \\
f_2^+(t) &= -\frac{4\overline{L}_9}{\sqrt{2}F^2} + \frac{1}{t} \sum_{I=1}^3 \left\{ (c_1^I - c_2^I) \left[2B_2^I(t) - \frac{(t + \Delta_I)\Delta_I J_I(t)}{2t} \right] - c_2^I \Delta_I J_I(t) \right\} \\
f_3^+(t) &= \frac{F_K}{\sqrt{2}F_\pi} + \frac{1}{2t} \sum_{I=1}^3 \left\{ (c_1^I + c_2^I)(t + \Delta_I) - 2c_3^I \right\} \Delta_I J_I(t) \\
\overline{L}_9 &= L_9^r(\mu) - \frac{1}{256\pi^2} \ln \frac{M_\pi M_K^2 M_\eta}{\mu^4} \\
\Delta_I &= M_I^2 - m_I^2, \quad t = (p - p')^2.
\end{aligned} \tag{4.20}$$

\overline{L}_9 is a scale independent coupling constant and we have traded the tadpole contribution together with L_5 for F_K/F_π in $f_3^+(t)$. The sum over I corresponds to the three loop diagrams of Fig. 4.2 with coefficients c_1^I, c_2^I, c_3^I displayed in table 4.3. We use the Gell-Mann–Okubo mass formula throughout to express M_η^2 in terms of M_K^2, M_π^2 . The functions $J_I(t)$ and $B_2^I(t)$ can be found in App. B.

The standard K_{l3} form factors $f_+(t), f_-(t)$ as given in the previous subsection [24] are

$$\begin{aligned}
f_+(t) &= \frac{1}{\sqrt{2}} f_1^+(t) \\
f_-(t) &= \frac{1}{\sqrt{2}} \left[(M_K^2 - M_\pi^2 - t)f_2^+(t) + 2f_3^+(t) - f_1^+(t) \right].
\end{aligned} \tag{4.21}$$

It remains to calculate the infrared finite tensor amplitude $\hat{V}_{\mu\nu}^+$. The invariant amplitudes V_i^+ can be expressed in terms of the previously defined functions f_i^+ and of additional amplitudes I_1, I_2, I_3 . Diagrammatically, the latter amplitudes arise from those diagrams in Fig. 4.2 where the photon is not appended on the incoming K^+ (non-Bremsstrahlung

diagrams). The final expressions are

$$\begin{aligned}
V_1^+ &= I_1 + p'W_q f_2^+(W_q^2) + f_3^+(W_q^2) \\
V_2^+ &= I_2 - \frac{1}{pq} [p'W_q f_2^+(W_q^2) + f_3^+(W_q^2)] \\
V_3^+ &= I_3 + \frac{1}{pq} [p'W f_2^+(W^2) + f_3^+(W^2) - p'W_q f_2^+(W_q^2) - f_3^+(W_q^2)] \\
V_4^+ &= \frac{f_1^+(W^2) - f_1^+(W_q^2)}{pq} \\
W_q &= W + q = p - p'.
\end{aligned} \tag{4.22}$$

The amplitudes I_1, I_2, I_3 in Eq.(4.22) are given by

$$\begin{aligned}
I_1 &= \frac{4qW}{\sqrt{2}F^2}(\overline{L_9} + \overline{L_{10}}) + \frac{8p'q}{\sqrt{2}F^2}\overline{L_9} \\
&\quad + \sum_{I=1}^3 \left\{ [(W_q^2 + \Delta_I)(c_1^I + c_2^I) - 2(c_2^I p'W_q + c_3^I)] \left[\frac{(W_q^2 - \Delta_I)\hat{J}_I}{2W_q^2} - 2G_I \right] \right. \\
&\quad + \frac{(c_2^I - c_1^I)}{2} \left[\frac{p'W_q}{W_q^2} \left(\frac{(W_q^4 - \Delta_I^2)\hat{J}_I}{W_q^2} + 4\hat{B}_2^I \right) + p'(W - q)L_m^I \right] \\
&\quad \left. + \frac{2(c_2^I - c_1^I)}{qW} [p'q(F_I - (W_q^2 + \Delta_I)G_I) + p'W(\hat{B}_2^I - B_2^I)] \right\} \\
I_2 &= -\frac{8\overline{L_9}}{\sqrt{2}F^2} + \frac{2}{qW} \sum_{I=1}^3 (c_2^I - c_1^I) [F_I - (W^2 + \Delta_I)G_I] \\
I_3 &= -\frac{4\overline{L_9}}{\sqrt{2}F^2} + \sum_{I=1}^3 \left\{ 2(c_2^I - c_1^I) \left[G_I + \frac{L_m^I}{4} + \frac{\hat{B}_2^I - B_2^I}{qW} \right] - c_1^I \frac{\Delta_I J_I}{W^2} \right\} \\
\overline{L_{10}} &= L_{10}^r(\mu) + \frac{1}{256\pi^2} \ln \frac{M_\pi M_K^2 M_\eta}{\mu^4} \\
L_m^I &= \frac{\Sigma_I}{32\pi^2 \Delta_I} \ln \frac{m_I^2}{M_I^2} \\
F_I &= \hat{B}_2^I - \frac{W^2}{4} L_m^I + \frac{1}{qW} (W^2 B_2^I - W_q^2 \hat{B}_2^I) \\
G_I &= \frac{M_I^2}{2} C(W_q^2, W^2, M_I^2, m_I^2) + \frac{1}{8qW} [(W_q^2 + \Delta_I)\hat{J}_I - (W^2 + \Delta_I)J_I] + \frac{1}{64\pi^2} \\
J_I &\equiv J_I(W^2), \quad \hat{J}_I \equiv J_I(W_q^2) \\
B_2^I &\equiv B_2^I(W^2), \quad \hat{B}_2^I \equiv B_2^I(W_q^2).
\end{aligned} \tag{4.23}$$

The function $C(W_q^2, W^2, M_I^2, m_I^2)$ is given in App. B. All the invariant amplitudes V_1^+, \dots, V_4^+ are real in the physical region. Of course, the same is true for the K_{l3} matrix element F_ν^+ .

Table 4.4: Coefficients for the $K_{l3\gamma}^0$ loop amplitudes corresponding to the diagrams $I = 1, 2, 3$ in Fig. 4.2. All coefficients c_i^I must be divided by $6\sqrt{2}F^2$.

I	M_I	m_I	c_1^I	c_2^I	c_3^I
1	M_K	M_π	0	-3	$-3M_K^2$
2	M_K	M_η	6	-3	$M_K^2 + 2M_\pi^2$
3	M_π	M_K	4	-2	$-2M_K^2 + 2M_\pi^2$

The $K_{l3\gamma}^0$ amplitude has a very similar structure. Both the K_{l3}^0 matrix element F_ν^0 and the infrared finite vector amplitude $\hat{V}_{\mu\nu}^0$ can be obtained from the corresponding quantities F_ν^+ and $\hat{V}_{\mu\nu}^+$ by the following steps:

- interchange p' and $-p$;
- replace $\frac{F_K}{F_\pi}$ by $\frac{F_\pi}{F_K}$ in f_3^+ ;
- insert the appropriate coefficients c_i^I for $K_{l3\gamma}^0$ listed in table 4.4;
- multiply F_ν^+ and $\hat{V}_{\mu\nu}^+$ by a factor $-\sqrt{2}$.

4.4.2 Numerical results

In calculating the rates with the complete amplitudes of the previous subsection, we use the same cuts as for the tree level rates in Subsect. 4.2:

$$\begin{aligned} E_\gamma &\geq 30 \text{ MeV} \\ \theta_{l\gamma} &\geq 20^\circ. \end{aligned} \tag{4.24}$$

The physical values of M_π and M_K are used in the amplitudes. M_η is calculated from the Gell-Mann–Okubo mass formula. The values of the other parameters can be found in Ref. [2] and in appendix A.

The results for $K_{l3\gamma}^+$ and $K_{l3\gamma}^0$ are displayed in tables 4.5 and 4.6, respectively. For comparison, the tree level branching ratios of table 4.1 and the rates for the amplitudes without the loop contributions are also shown. The separation between loop and counter-term contributions is of course scale dependent. This scale dependence is absorbed in the scale invariant constants $\overline{L}_9, \overline{L}_{10}$ defined in Eqs.(4.20), (4.23). In other words, the entries in tables 4.5, 4.6 for the amplitudes without loops correspond to setting all coefficients c_i^I in tables 4.3, 4.4 equal to zero.

Table 4.5: Branching ratios and expected number of events at DAΦNE for $K_{l3\gamma}^+$.

$K_{e3\gamma}^+$	BR	#events/yr
full $O(p^4)$ amplitude	3.0×10^{-4}	2.7×10^6
tree level	2.8×10^{-4}	2.5×10^6
$O(p^4)$ without loops	3.2×10^{-4}	2.9×10^6

$K_{\mu3\gamma}^+$	BR	#events/yr
full $O(p^4)$ amplitude	2.0×10^{-5}	1.8×10^5
tree level	1.9×10^{-5}	1.7×10^5
$O(p^4)$ without loops	2.1×10^{-5}	1.9×10^5

Table 4.6: Branching ratios and expected number of events at DAΦNE for $K_{l3\gamma}^0$.

$K_{e3\gamma}^0$	BR	#events/yr
full $O(p^4)$ amplitude	3.8×10^{-3}	4.2×10^6
tree level	3.6×10^{-3}	4.0×10^6
$O(p^4)$ without loops	4.0×10^{-3}	4.4×10^6

$K_{\mu3\gamma}^0$	BR	#events/yr
full $O(p^4)$ amplitude	5.6×10^{-4}	6.1×10^5
tree level	5.2×10^{-4}	5.7×10^5
$O(p^4)$ without loops	5.9×10^{-4}	6.5×10^5

4.5 Improvements at DAΦNE

The numerical results given above demonstrate very clearly that the non-trivial CHPT effects of $O(p^4)$ can be detected at DAΦNE in all four channels without any problem of statistics. Of course, the rates are bigger for the electronic modes. On the other hand, the relative size of the structure dependent terms is somewhat bigger in the muonic channels (around 8% for the chosen cuts). We observe that there is negative interference between the loop and counterterm amplitudes.

The sensitivity to the counterterm coupling constants L_9, L_{10} and to the chiral anomaly can be expressed as the difference in the number of events between the tree level and the $O(p^4)$ amplitudes (without loops). In the optimal case of $K_{e3\gamma}^0$, this amounts to more than 4×10^5 events/yr at DAΦNE. Almost all of this difference is due to L_9 . It will be very difficult to extract the coupling constant L_{10} from the total rates. A more detailed study is needed to determine whether L_{10} can be extracted from differential distributions.

The chiral anomaly is more important for $K_{l3\gamma}^+$, but even there it influences the total rates rather little. Once again, a dedicated study of differential rates is necessary to locate the chiral anomaly, if possible at all.

On the other hand, taking into account that L_9 is already known to good accuracy (see table 1 in Ref. [2]), $K_{l3\gamma}$ decays will certainly allow for precise and unambiguous tests of the one-loop effects in CHPT [11].

5 K_{l4} decays

In this subsection we discuss the decays

$$K^+(p) \rightarrow \pi^+(p_1) \pi^-(p_2) l^+(p_l) \nu_l(p_\nu) \quad (5.1)$$

$$K^+(p) \rightarrow \pi^0(p_1) \pi^0(p_2) l^+(p_l) \nu_l(p_\nu) \quad (5.2)$$

$$K^0(p) \rightarrow \pi^0(p_1) \pi^-(p_2) l^+(p_l) \nu_l(p_\nu) \quad (5.3)$$

and their charge conjugate modes. The letter l stands for e or μ . We do not consider isospin violating contributions and correspondingly set $m_u = m_d$, $\alpha = 0$.

5.1 Kinematics

We start with the process (5.1). The full kinematics of this decay requires five variables. We will use the ones introduced by Cabibbo and Maksymowicz [51]. It is convenient to consider three reference frames, namely the K^+ rest system (Σ_K), the $\pi^+\pi^-$ center-of-mass system ($\Sigma_{2\pi}$) and the $l^+\nu_l$ center-of-mass system ($\Sigma_{l\nu}$). Then the variables are

1. s_π , the effective mass squared of the dipion system,

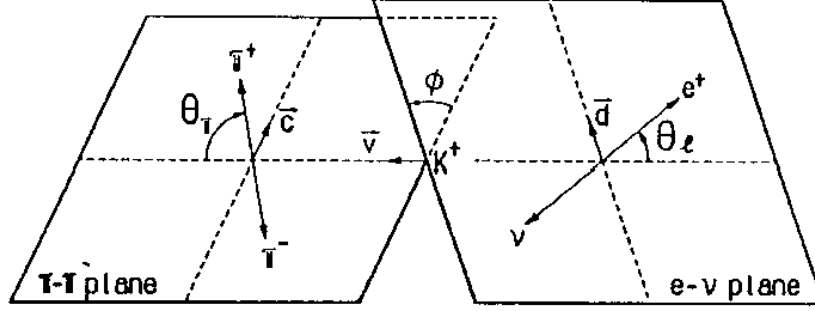


Figure 5.1: Kinematic variables for K_{l4} decays. The angle θ_π is defined in $\Sigma_{2\pi}$, θ_l in $\Sigma_{l\nu}$ and ϕ in Σ_K .

2. s_l , the effective mass squared of the dilepton system,
3. θ_π , the angle of the π^+ in $\Sigma_{2\pi}$ with respect to the dipion line of flight in Σ_K ,
4. θ_l , the angle of the l^+ in $\Sigma_{l\nu}$ with respect to the dilepton line of flight in Σ_K , and
5. ϕ , the angle between the plane formed by the pions in Σ_K and the corresponding plane formed by the dileptons.

The angles θ_π , θ_l and ϕ are displayed in Fig. 5.1. In order to specify these variables more precisely, let \vec{p}_1 be the three-momentum of the π^+ in $\Sigma_{2\pi}$ and \vec{p}_l the three-momentum of the l^+ in $\Sigma_{l\nu}$. Furthermore, let \vec{v} be a unit vector along the direction of flight of the dipion in Σ_K , and $\vec{c}(\vec{d})$ a unit vector along the projection of \vec{p}_1 (\vec{p}_l) perpendicular to \vec{v} ($-\vec{v}$),

$$\begin{aligned}\vec{c} &= (\vec{p}_1 - \vec{v}\vec{v} \cdot \vec{p}_1) / [\vec{p}_1^2 - (\vec{p}_1 \cdot \vec{v})^2]^{1/2} \\ \vec{d} &= (\vec{p}_l - \vec{v}\vec{v} \cdot \vec{p}_l) / [\vec{p}_l^2 - (\vec{p}_l \cdot \vec{v})^2]^{1/2} .\end{aligned}$$

The vectors \vec{v} , \vec{c} and \vec{d} are indicated in Fig. 5.1. Then, one has

$$\begin{aligned}s_\pi &= (p_1 + p_2)^2, \quad s_l = (p_l + p_\nu)^2 \\ \cos \theta_\pi &= \vec{v} \cdot \vec{p}_1 / |\vec{p}_1|, \quad \cos \theta_l = -\vec{v} \cdot \vec{p}_l / |\vec{p}_l| \\ \cos \phi &= \vec{c} \cdot \vec{d}, \quad \sin \phi = (\vec{c} \times \vec{v}) \cdot \vec{d}.\end{aligned}\tag{5.4}$$

The range of the variables is

$$\begin{aligned}4M_\pi^2 &\leq s_\pi \leq (M_K - m_l)^2 \\ m_l^2 &\leq s_l \leq (M_K - \sqrt{s_\pi})^2 \\ 0 &\leq \theta_\pi, \theta_l \leq \pi, \quad 0 \leq \phi \leq 2\pi.\end{aligned}\tag{5.5}$$

It is useful to furthermore introduce the following combinations of four vectors

$$P = p_1 + p_2, \quad Q = p_1 - p_2, \quad L = p_l + p_\nu, \quad N = p_l - p_\nu \quad (5.6)$$

together with the corresponding Lorentz invariant scalar products

$$\begin{aligned} P^2 &= s_\pi, \quad Q^2 = 4M_\pi^2 - s_\pi, \quad L^2 = s_l, \quad N^2 = 2m_l^2 - s_l, \\ PQ &= 0, \\ PL &= \frac{1}{2}(M_K^2 - s_\pi - s_l), \\ PN &= z_l PL + (1 - z_l)X \cos \theta_l, \\ QL &= \sigma_\pi X \cos \theta_\pi, \\ QN &= z_l QL + \sigma_\pi(1 - z_l)[PL \cos \theta_\pi \cos \theta_l \\ &\quad - (s_\pi s_l)^{1/2} \sin \theta_\pi \sin \theta_l \cos \phi] \\ LN &= m_l^2 \\ \langle LNPQ \rangle &\equiv \epsilon_{\mu\nu\rho\sigma} L^\mu N^\nu P^\rho Q^\sigma \\ &= -(s_\pi s_l)^{1/2} \sigma_\pi(1 - z_l)X \sin \theta_\pi \sin \theta_l \sin \phi \end{aligned} \quad (5.7)$$

with

$$\begin{aligned} X &= ((PL)^2 - s_\pi s_l)^{1/2} = \frac{1}{2}\lambda^{1/2}(M_K^2, s_\pi, s_l) \\ z_l &= m_l^2/s_l \\ \sigma_\pi &= (1 - 4M_\pi^2/s_\pi)^{1/2}. \end{aligned} \quad (5.8)$$

Below we will also use the variables

$$\begin{aligned} t &= (p_1 - p)^2 \\ u &= (p_2 - p)^2. \end{aligned} \quad (5.9)$$

These are related to s_π, s_l and θ_π by

$$\begin{aligned} t + u &= 2M_\pi^2 + M_K^2 + s_l - s_\pi \\ t - u &= -2\sigma_\pi X \cos \theta_\pi. \end{aligned} \quad (5.10)$$

5.2 Matrix elements

The matrix element for $K^+ \rightarrow \pi^+ \pi^- l^+ \nu_l$ is

$$T = \frac{G_F}{\sqrt{2}} V_{us}^* \bar{u}(p_\nu) \gamma_\mu (1 - \gamma_5) v(p_l) (V^\mu - A^\mu) \quad (5.11)$$

where

$$\begin{aligned}
I_\mu &= \langle \pi^+(p_1)\pi^-(p_2)\text{out} | I_\mu^{4-i5}(0) | K^+(p) \rangle; \quad I = V, A \\
V_\mu &= -\frac{H}{M_K^3} \epsilon_{\mu\nu\rho\sigma} L^\nu P^\rho Q^\sigma \\
A_\mu &= -i\frac{1}{M_K} [P_\mu F + Q_\mu G + L_\mu R]
\end{aligned} \tag{5.12}$$

and $\epsilon_{0123} = 1$. The matrix elements for the other channels (5.2,5.3) may be obtained from (5.11,5.12) by isospin symmetry, see below.

The form factors F, G, R and H are real analytic functions of the three variables $p_1 p_2$, $p_1 p$ and $p_2 p$. Below, we will use instead the variables $\{s_\pi, s_l, \theta_\pi\}$ or $\{s_\pi, t, u\}$.

Remark: In order to agree with the notation used by Pais and Treiman [52] and by Rosset et al. [53], we have changed our previous convention [54, 55] in the definition of the anomaly form factor H . See also the comments after Eq. (5.21).

5.3 Decay rates

The partial decay rate for (5.1) is given by

$$d\Gamma = \frac{1}{2M_K(2\pi)^8} \sum_{spins} |T|^2 d_{LIPS}(p; p_l, p_\nu, p_1, p_2). \tag{5.13}$$

The quantity $\sum_{spins} |T|^2$ is a Lorentz invariant quadratic form in F, G, R and H . All scalar products can be expressed in the 5 independent variables $s_\pi, s_l, \theta_\pi, \theta_l$ and ϕ , such that

$$\sum_{spins} |T|^2 = 2G_F^2 |V_{us}|^2 M_K^{-2} J_5(s_\pi, s_l, \theta_\pi, \theta_l, \phi). \tag{5.14}$$

Carrying out the integrations over the remaining $4 \cdot 3 - 5 = 7$ variables in (5.13) gives [51]

$$d\Gamma_5 = G_F^2 |V_{us}|^2 N(s_\pi, s_l) J_5(s_\pi, s_l, \theta_\pi, \theta_l, \phi) ds_\pi ds_l d(\cos \theta_\pi) d(\cos \theta_l) d\phi \tag{5.15}$$

where

$$N(s_\pi, s_l) = (1 - z_l) \sigma_\pi X / (2^{13} \pi^6 M_K^5). \tag{5.16}$$

The form factors F, G, R and H are independent of ϕ and θ_l . It is therefore possible to carry out two more integrations in (5.15) with the result

$$d\Gamma_3 = G_F^2 |V_{us}|^2 N(s_\pi, s_l) J_3(s_\pi, s_l, \theta_\pi) ds_\pi ds_l d(\cos \theta_\pi). \tag{5.17}$$

The explicit form of J_5 is

$$\begin{aligned}
J_5 = & |F|^2 \left[(PL)^2 - (PN)^2 - s_\pi s_l + m_l^2 s_\pi \right] \\
& + |G|^2 \left[(QL)^2 - (QN)^2 - Q^2 s_l + m_l^2 Q^2 \right] \\
& + |R|^2 m_l^2 \left[s_l - m_l^2 \right] \\
& + \frac{1}{M_K^4} |H|^2 \left[(m_l^2 - s_l) \left[Q^2 X^2 + s_\pi (QL)^2 \right] - \langle LNPQ \rangle^2 \right] \\
& + (F^* G + F G^*) [(PL)(QL) - (PN)(QN)] \\
& + (F^* R + F R^*) m_l^2 [(PL) - (PN)] \\
& + \frac{1}{M_K^2} (F^* H + F H^*) \left[(QN)(PL)^2 - (QL)(PL)(PN) - s_\pi s_l (QN) + m_l^2 s_\pi (QL) \right] \\
& + (G^* R + G R^*) m_l^2 [(QL) - (QN)] \\
& + \frac{1}{M_K^2} (G^* H + G H^*) \left[(PL)(QL)(QN) - (PN)(QL)^2 + s_l (PN) Q^2 - m_l^2 (PL) Q^2 \right] \\
& + \frac{i}{M_K^2} \langle LNPQ \rangle \left[-(F^* G - F G^*) M_K^2 + (F^* H - F H^*) (PN) \right. \\
& \left. + (G^* H - G H^*) (QN) + (R^* H - R H^*) m_l^2 \right] .
\end{aligned} \tag{5.18}$$

For data analysis it is useful to represent this result in a still different form which displays the θ_l and ϕ dependence more clearly [52]:

$$\begin{aligned}
J_5 = & 2(1 - z_l) \left[I_1 + I_2 \cos 2\theta_l + I_3 \sin^2 \theta_l \cdot \cos 2\phi + I_4 \sin 2\theta_l \cdot \cos \phi + I_5 \sin \theta_l \cdot \cos \phi \right. \\
& \left. + I_6 \cos \theta_l + I_7 \sin \theta_l \cdot \sin \phi + I_8 \sin 2\theta_l \cdot \sin \phi + I_9 \sin^2 \theta_l \cdot \sin 2\phi \right] .
\end{aligned} \tag{5.19}$$

One obtains

$$\begin{aligned}
I_1 &= \frac{1}{4} \left\{ (1 + z_l) |F_1|^2 + \frac{1}{2} (3 + z_l) \left(|F_2|^2 + |F_3|^2 \right) \sin^2 \theta_\pi + 2z_l |F_4|^2 \right\} \\
I_2 &= -\frac{1}{4} (1 - z_l) \left\{ |F_1|^2 - \frac{1}{2} \left(|F_2|^2 + |F_3|^2 \right) \sin^2 \theta_\pi \right\} \\
I_3 &= -\frac{1}{4} (1 - z_l) \left\{ |F_2|^2 - |F_3|^2 \right\} \sin^2 \theta_\pi \\
I_4 &= \frac{1}{2} (1 - z_l) \operatorname{Re}(F_1^* F_2) \sin \theta_\pi \\
I_5 &= -\left\{ \operatorname{Re}(F_1^* F_3) + z_l \operatorname{Re}(F_4^* F_2) \right\} \sin \theta_\pi \\
I_6 &= -\left\{ \operatorname{Re}(F_2^* F_3) \sin^2 \theta_\pi - z_l \operatorname{Re}(F_1^* F_4) \right\} \\
I_7 &= -\left\{ \operatorname{Im}(F_1^* F_2) + z_l \operatorname{Im}(F_4^* F_3) \right\} \sin \theta_\pi
\end{aligned}$$

$$\begin{aligned}
I_8 &= \frac{1}{2}(1 - z_l) \operatorname{Im}(F_1^* F_3) \sin \theta_\pi \\
I_9 &= -\frac{1}{2}(1 - z_l) \operatorname{Im}(F_2^* F_3) \sin^2 \theta_\pi ,
\end{aligned} \tag{5.20}$$

where

$$\begin{aligned}
F_1 &= X \cdot F + \sigma_\pi(PL) \cos \theta_\pi \cdot G \\
F_2 &= \sigma_\pi(s_\pi s_l)^{1/2} G \\
F_3 &= \sigma_\pi X (s_\pi s_l)^{1/2} \frac{H}{M_K^2} \\
F_4 &= -(PL)F - s_l R - \sigma_\pi X \cos \theta_\pi \cdot G .
\end{aligned} \tag{5.21}$$

The definition of F_1, \dots, F_4 in (5.21) corresponds to the combinations used by Pais and Treiman [52] (the different sign in the terms $\sim PL$ is due to our use of the metric $\operatorname{diag}(+ - - -)$). The form factors I_1, \dots, I_9 agree with the expressions given in [52]. We conclude that our convention for the relative phase in the definition of the form factors in Eq. (5.12) agrees with the one used by Pais and Treiman. The comparison of (5.18) with [53, table II] shows furthermore that it also agrees with this reference.

The quantity J_3 can now easily be obtained from (5.19) by integrating over ϕ and θ_l ,

$$J_3 = \int d\phi d(\cos \theta_l) J_5 = 8\pi(1 - z_l) \left[I_1 - \frac{1}{3} I_2 \right]. \tag{5.22}$$

5.4 Isospin decomposition

The K_{l4} decays (5.2) and (5.3) involve the same form factors as displayed in Eq. (5.12). We denote by A_{+-} , A_{00} and A_{0-} the current matrix elements of the processes (5.1)-(5.3). These are related by isospin symmetry ⁶,

$$A_{+-} = \frac{A_{0-}}{\sqrt{2}} - A_{00} . \tag{5.23}$$

This relation also holds for the individual form factors, which may be decomposed into a symmetric and an antisymmetric part under $t \leftrightarrow u$ ($p_1 \leftrightarrow p_2$). Because of Bose symmetry and of the $\Delta I = \frac{1}{2}$ rule of the relevant weak currents, one has

$$\begin{aligned}
(F, G, R, H)_{00} &= -(F^+, G^-, R^+, H^-)_{+-} \\
(F, G, R, H)_{0-} &= \sqrt{2}(F^-, G^+, R^-, H^+)_{+-}
\end{aligned} \tag{5.24}$$

where

$$F_{+-}^\pm = \frac{1}{2}[F(s_\pi, t, u) \pm F(s_\pi, u, t)] \tag{5.25}$$

⁶We use the Condon-Shortley phase conventions.

and $F(s_\pi, t, u)$ is defined in Eq. (5.12).

The isospin relation for the decay rates is

$$\Gamma(K^+ \rightarrow \pi^+ \pi^- l^+ \nu_l) = \frac{1}{2} \Gamma(K_L \rightarrow \pi^0 \pi^\pm l^\mp \nu) + 2 \Gamma(K^+ \rightarrow \pi^0 \pi^0 l^+ \nu_l) . \quad (5.26)$$

Isospin violating contributions affect the matrix elements and phase space, as a result of which this relation is modified. In order to illustrate the (substantial) effects from asymmetries in phase space, we take constant form factors F, G and set $R = 0, H = 0$. Eq. (5.26) then reads (with physical masses for $K^+ \rightarrow \pi^+ \pi^- l^+ \nu_l, \pi^0 \pi^0 l^+ \nu_l$ and with $M_{\pi^0} = M_{\pi^\pm} = 137$ MeV in $K_L \rightarrow \pi^0 \pi^\mp l^\pm \nu$)

$$\begin{aligned} (16.0F^2 + 3.1G^2)\Gamma_0 &= (20.1F^2 + 2.0G^2)\Gamma_0 \\ \Gamma_0 &= V_{us}^2 \cdot 10^2 \text{sec}^{-1} \end{aligned} \quad (5.27)$$

in the electron mode and

$$(1.79F^2 + 0.25G^2)\Gamma_0 = (2.64F^2 + 0.20G^2)\Gamma_0 \quad (5.28)$$

in the muon mode.

5.5 Partial wave expansion

The form factors may be written in a partial wave expansion in the variable θ_π . We consider a definite isospin $\pi\pi$ state. Suppressing isospin indices, one has [56, 57]

$$\begin{aligned} F &= \sum_{l=0}^{\infty} P_l(\cos \theta_\pi) f_l - \frac{\sigma_\pi PL}{X} \cos \theta_\pi G \\ G &= \sum_{l=1}^{\infty} P'_l(\cos \theta_\pi) g_l \\ R &= \sum_{l=0}^{\infty} P_l(\cos \theta_\pi) r_l + \frac{\sigma_\pi s_\pi}{X} \cos \theta_\pi G \\ H &= \sum_{l=0}^{\infty} P'_l(\cos \theta_\pi) h_l \end{aligned} \quad (5.29)$$

where

$$P'_l(z) = \frac{d}{dz} P_l(z) . \quad (5.30)$$

The partial wave amplitudes f_l, g_l, r_l and h_l depend on s_π and s_l . Their phase coincides with the phase shifts δ_l^I in elastic $\pi\pi$ scattering (angular momentum l , isospin I). More precisely, the quantities

$$\begin{aligned} e^{-i\delta_{2l}^0} X_{2l} \\ e^{-i\delta_{2l+1}^1} X_{2l+1} ; l = 0, 1, \dots ; X = f, g, r, h \end{aligned} \quad (5.31)$$

Table 5.1: Rates of K_{l4} decays [3]. The data for $K_L \rightarrow \pi^0 \pi^\pm e^\mp \nu$ is from ref. [60].

	branching ratio	‡ events		improve- ment
		Particle Data Group	DAΦNE 1 yr	
$K^+ \rightarrow \pi^+ \pi^- e^+ \nu_e$	$3.91 \cdot 10^{-5}$	$3 \cdot 10^4$	$3 \cdot 10^5$	10
$K^+ \rightarrow \pi^0 \pi^0 e^+ \nu_e$	$2.1 \cdot 10^{-5}$	< 50	$2 \cdot 10^5$	$> 4 \cdot 10^3$
$K_L \rightarrow \pi^0 \pi^\pm e^\mp \nu$	$5.16 \cdot 10^{-5}$	729	$7 \cdot 10^4$	$7 \cdot 10^2$
$K^+ \rightarrow \pi^+ \pi^- \mu^+ \nu_\mu$	10^{-6}	7	$2 \cdot 10^4$	$3 \cdot 10^3$

are real in the physical region of K_{l4} decay. The form factors F_1 and F_4 therefore have a simple expansion

$$\begin{aligned}
F_1 &= X \sum_l P_l(\cos \theta_\pi) f_l \\
F_4 &= - \sum_l P_l(\cos \theta_\pi) (PL f_l + s_l r_l).
\end{aligned} \tag{5.32}$$

On the other hand, the phase of the projected amplitudes

$$F_{2l} = \int P_l(\cos \theta_\pi) F_2 d(\cos \theta_\pi) ; l = 0, 1, 2, \dots \tag{5.33}$$

is not given by δ_l^I , e.g., $e^{-i\delta_1^1} F_{20}$ is not real in the isospin one case. A similar remark applies to F_3 .

5.6 Previous experiments

We display in table 5.1 the number of events collected so far. The data are obviously dominated by the work of Rosselet et al. [53], which measures the $\pi^+ \pi^-$ final state with good statistics. The authors parametrize the form factors as

$$\begin{aligned}
F &= f_s e^{i\delta_0^0} + f_p e^{i\delta_1^1} \cos \theta_\pi + \text{D-wave} \\
G &= g e^{i\delta_1^1} + \text{D-wave} \\
H &= h e^{i\delta_1^1} + \text{D-wave}
\end{aligned} \tag{5.34}$$

with f_s, f_p, g and h assumed to be real ⁷. Furthermore, they put $m_e = 0$, such that the form factors R and F_4 drop out in the decay distribution. Despite the good statistics, the

⁷Note that, according to what is said in the previous subsection, the terms denoted by "D-wave" in Eq. (5.34) all contain (complex) contributions which are proportional to $P_l(\cos \theta_\pi)$, $l \geq 0$.

experiment has not been able to separate out the full kinematic behaviour of the matrix elements. Therefore certain approximations/assumptions had to be made. For example, no dependence on s_l was seen within the limits of the data, so that the results were quoted assuming that such a dependence is absent. Similarly, f_p was found to be compatible with zero, and hence put equal to zero when the final result for g was derived. A dependence on s_π was seen, and found to be compatible with

$$\begin{aligned} f_s(q^2) &= f_s(0)[1 + \lambda_f q^2] \\ g(q^2) &= g(0)[1 + \lambda_g q^2] \\ h(q^2) &= h(0)[1 + \lambda_h q^2] \\ q^2 &= (s_\pi - 4M_\pi^2)/4M_\pi^2 \end{aligned} \quad (5.35)$$

with

$$\lambda_f = \lambda_g = \lambda_h = \lambda. \quad (5.36)$$

These approximations to the form factors do not agree completely with what is found in the theoretical predictions. Dependence on s_l and non-zero values for higher partial waves all occur in the theoretical results.

The experimental results for the threshold values and the slopes of the form factors are [53]

$$\begin{aligned} f_s(0) &= 5.59 \pm 0.14 \\ g(0) &= 4.77 \pm 0.27 \\ h(0) &= -2.68 \pm 0.68 \\ \lambda &= 0.08 \pm 0.02. \end{aligned} \quad (5.37)$$

We have used [3] $|V_{us}| = 0.22$ in transcribing these results. (We note that from Eqs. (5.34 - 5.37) and $f_p = 0$ we obtain $\Gamma_{K_{e4}} = (2.94 \pm 0.16) \cdot 10^3 \text{ sec}^{-1}$. This value must be compared with $\Gamma_{K_{e4}} = (3.26 \pm 0.15) \cdot 10^3 \text{ sec}^{-1}$ obtained in the same experiment.) In addition to the threshold values (5.37) of the form factors, the phase shift difference $\delta = \delta_0^0 - \delta_1^1$ was determined [53] in five energy bins. The S-wave scattering length a_0^0 was then extracted by using a model of Basdevant, Froggatt and Petersen [58]. This model is based on solutions to Roy equations. The result for the scattering length is

$$a_0^0 = 0.28 \pm 0.05. \quad (5.38)$$

A study by [59], based on a more recent solution to Roy equations, gives

$$a_0^0 = 0.26 \pm 0.05. \quad (5.39)$$

Turning now to the $\pi^0 \pi^\pm e^\mp \nu_e$ channel, we consider the following recent data (based on 729 ± 15 events) [60]:

$$BR(K_L \rightarrow \pi^0 \pi^\mp e^\pm \nu) = (5.16 \pm 0.2 \pm 0.22) \cdot 10^{-5}. \quad (5.40)$$

The group also measured the G form factor. Defining

$$G_{0-} = G_0(1 + \lambda_g q^2) e^{i\delta_1^1} , \quad (5.41)$$

they find

$$\begin{aligned} G_0 &= 7.8 \pm 0.7 \pm 0.2 , \\ \lambda_g &= 0.014 \pm 0.087 \pm 0.070 . \end{aligned} \quad (5.42)$$

The slope agrees within the errors with the value (5.37) found by Rosselet et al. [53]. To compare the value of the form factor at threshold, we use the isospin prediction

$$|g(0)| = |G_0|/\sqrt{2} = 5.5 \pm 0.5 , \quad (5.43)$$

which is not incompatible with $g(0) = 4.77 \pm 0.27$ in eq. (5.37). (Here we have used $|V_{us}| = 0.22$ to transcribe the data. Furthermore, we assume that the form factor G_{0-} measured in Ref. [60] indeed has to be divided by $\sqrt{2}$ for the comparison with [53]. This is not quite clear to us reading [60].)

Finally for the channel $\pi^0 \pi^0 e^+ \nu_e$, we consider the rate [3]

$$\Gamma_{K^+ \rightarrow \pi^0 \pi^0 e^+ \nu_e} = \left(1.70_{-0.29}^{+0.34}\right) \cdot 10^3 \text{sec}^{-1} . \quad (5.44)$$

The kinematic dependence of the form factors on the variables s_π, s_l and θ_π has not yet been resolved experimentally in this decay. In order to proceed, we assume that the form factors in this channel are independent of θ_π , e.g., $F_{00} = F_{00}(s_\pi, t + u)$ etc. As a result of this assumption, G_{00} and H_{00} vanish by Bose statistics. The contribution from R_{00} is completely negligible in the electron mode, and the contribution from the anomaly form factor to the decay (5.44) is tiny. We neglect it altogether, as a result of which the above decay is fully determined by F_{00} . We write

$$F_{00} = F_0(1 + \lambda q^2) e^{i\delta_0^0} , \quad (5.45)$$

and obtain for the rate

$$2\Gamma_{K^+ \rightarrow \pi^0 \pi^0 e^+ \nu_e} = |F_0 V_{us}|^2 (2.01 + 1.7\lambda + O(\lambda^2)) \cdot 10^3 \text{sec}^{-1} . \quad (5.46)$$

This finally gives with $\lambda = 0.08$

$$|F_0| = 5.72_{-0.49}^{+0.57} , \quad (5.47)$$

which compares very well with the isospin prediction

$$|F_0| = |f_s(0)| = 5.59 \pm 0.14 . \quad (5.48)$$

5.7 Theory

The theoretical predictions of K_{l4} form factors have a long history which started in the sixties with the current algebra evaluation of F , G , R and H . For an early review of the subject and for references to work prior to CHPT we refer the reader to [34] (see also [35]). Here we concentrate on the evaluation of the form factors in the framework of CHPT [54, 55, 61, 62].

5.7.1 Form factors at tree level

The chiral representation of the form factors at leading order was originally given by Weinberg [63],

$$\begin{aligned} F &= G = \frac{M_K}{\sqrt{2}F_\pi} = 3.74 \ , \\ R &= \frac{M_K}{2\sqrt{2}F_\pi} \left(\frac{s_\pi + \nu}{s_l - M_K^2} + 1 \right) \ , \\ H &= 0 \ . \end{aligned} \tag{5.49}$$

The next-to-leading order corrections are displayed below, and the later sections contain an estimate of yet higher-order contributions. Here we note that the total decay rates which follow from Eq. (5.49) are typically a factor of two (ore more) below the data. As an example, consider the channel $K^+ \rightarrow \pi^+\pi^-e^+\nu_e$. Using (5.49), the total decay rate becomes⁸ 1297 sec^{-1} , whereas the experimental value is $3160 \pm 140 \text{ sec}^{-1}$ [3].

5.7.2 Form factors at one loop

The one-loop result for F [54],[55] may be written in the form

$$F(s_\pi, t, u) = \frac{M_K}{\sqrt{2}F_\pi} \left\{ 1 + \frac{1}{F_\pi^2} (U_F + P_F + C_F) + O(E^4) \right\} \ . \tag{5.50}$$

The contribution $U_F(s_\pi, t, u)$ denotes the unitarity correction generated by the one-loop graphs which appear at order E^4 in the low-energy expansion. Its expression will be given in appendix D.

The contribution $P_F(s_\pi, t, u)$ is a polynomial in s_π, t, u obtained from the tree graphs at order E^4 . We find

$$P_F(s_\pi, t, u) = \sum_{i=1}^9 p_{i,F}(s_\pi, t, u) L_i^r \ , \tag{5.51}$$

⁸If not stated otherwise, we use $F_\pi = 93.2 \text{ MeV}$, $|V_{us}| = 0.22$ and $(M_\pi, M_K) = (139.6, 493.6) \text{ MeV}$, $(135, 493.6) \text{ MeV}$ and $(137, 497.7) \text{ MeV}$ for the decays (5.1), (5.2) and (5.3), respectively.

where

$$\begin{aligned}
p_{1,F} &= 32(s_\pi - 2M_\pi^2) , \\
p_{2,F} &= 8(M_K^2 + s_\pi - s_l) , \\
p_{3,F} &= 4(M_K^2 - 3M_\pi^2 + 2s_\pi - t) , \\
p_{4,F} &= 32M_\pi^2 , \\
p_{5,F} &= 4M_\pi^2 , \\
p_{9,F} &= 2s_l .
\end{aligned} \tag{5.52}$$

The remaining coefficients $p_{i,F}$ are zero.

The contributions C_F contain logarithmic terms, independent of s_π, t and u :

$$C_F = \frac{1}{256\pi^2} \left[5M_\pi^2 \ln \frac{M_\pi^2}{\mu^2} - 2M_K^2 \ln \frac{M_K^2}{\mu^2} - 3M_\eta^2 \ln \frac{M_\eta^2}{\mu^2} \right] . \tag{5.53}$$

The corresponding decomposition of the form factor G is [54],[55]

$$G(s_\pi, t, u) = \frac{M_K}{\sqrt{2}F_\pi} \left\{ 1 + \frac{1}{F_\pi^2} (U_G + P_G + C_G) + O(E^4) \right\} , \tag{5.54}$$

For the expression of U_G see appendix D. The polynomials

$$P_G = \sum_{i=1}^9 p_{i,G}(s_\pi, t, u) L_i^r \tag{5.55}$$

are

$$\begin{aligned}
p_{2,G} &= 8(t - u) , \\
p_{3,G} &= 4(t - M_K^2 - M_\pi^2) , \\
p_{5,G} &= 4M_\pi^2 , \\
p_{9,G} &= 2s_l ,
\end{aligned} \tag{5.56}$$

The remaining $p_{i,G}$ vanish. The logarithms contained in C_G are

$$C_G = -C_F. \tag{5.57}$$

The form factor R contains a pole part $Z(s_\pi, t, u)/(s_l - M_K^2)$ and a regular piece Q . [Since the axial current acts as an interpolating field for a kaon, the residue of the pole part is related to the $KK \rightarrow \pi\pi$ amplitude in the standard manner.] We write

$$\begin{aligned}
R &= \frac{M_K}{2\sqrt{2}F_\pi} \left\{ \frac{Z}{s_l - M_K^2} + Q + O(E^4) \right\} , \\
I &= B_I + \frac{1}{F_\pi^2} (U_I + P_I + C_I) , \quad I = Z, Q .
\end{aligned} \tag{5.58}$$

According to (5.49), the Born terms B_I are [63]

$$\begin{aligned} B_Z &= s_\pi + \nu , \\ B_Q &= 1. \end{aligned} \quad (5.59)$$

The one-loop corrections have been worked out in Ref. [62]. The unitarity corrections U_I are displayed in the appendix D. The residues P_Z and C_Z are

$$P_Z(s_\pi, t, u) = \sum_{i=1}^9 p_{i,Z}(s_\pi, t, u) L_i^r , \quad (5.60)$$

with

$$\begin{aligned} p_{1,Z} &= 32(s_\pi - 2M_K^2)(s_\pi - 2M_\pi^2) , \\ p_{2,Z} &= 8(s_\pi^2 + \nu^2) , \\ p_{3,Z} &= -2 \left[2(\nu + 4\Sigma)s_\pi - 5s_\pi^2 - \nu^2 - 16M_K^2 M_\pi^2 \right] , \\ p_{4,Z} &= 32 \left[\Sigma s_\pi - 4M_K^2 M_\pi^2 \right] , \\ p_{5,Z} &= 4 \left[(s_\pi + \nu)\Sigma - 8M_K^2 M_\pi^2 \right] , \\ p_{6,Z} &= 128M_K^2 M_\pi^2 , \\ p_{8,Z} &= 64M_K^2 M_\pi^2 , \\ \Sigma &= M_K^2 + M_\pi^2 . \end{aligned} \quad (5.61)$$

The remaining $p_{i,Z}$ vanish. The logarithms in C_Z are

$$C_Z = -\frac{M_K^2 - M_\pi^2}{128\pi^2} \left[3M_\pi^2 \ln \frac{M_\pi^2}{\mu^2} - 2M_K^2 \ln \frac{M_K^2}{\mu^2} - M_\eta^2 \ln \frac{M_\eta^2}{\mu^2} \right] . \quad (5.62)$$

For the nonpole part Q we find:

$$P_Q(s_\pi, t, u) = \sum_{i=1}^9 p_{i,Q}(s_\pi, t, u) L_i^r , \quad (5.63)$$

with

$$\begin{aligned} p_{1,Q} &= 32(s_\pi - 2M_\pi^2) , \\ p_{2,Q} &= 8(M_K^2 - s_l) , \\ p_{3,Q} &= 2 \left[4(s_\pi - 2M_\pi^2) + M_K^2 - s_l \right] , \\ p_{4,Q} &= 32M_\pi^2 , \\ p_{5,Q} &= 4\Sigma , \\ p_{9,Q} &= 2 \left[(s_\pi + \nu) - (M_K^2 - s_l) \right] . \end{aligned} \quad (5.64)$$

The remaining $p_{i,Q}$ vanish. The logarithms in C_Q are

$$C_Q = \frac{1}{128\pi^2} \left[5M_\pi^2 \ln \frac{M_\pi^2}{\mu^2} - 2M_K^2 \ln \frac{M_K^2}{\mu^2} - 3M_\eta^2 \ln \frac{M_\eta^2}{\mu^2} \right] . \quad (5.65)$$

The first nonvanishing contribution in the chiral expansion of the form factor H is due to the chiral anomaly [12]. The prediction is [64]

$$H = -\frac{\sqrt{2}M_K^3}{8\pi^2 F_\pi^3} = -2.66 , \quad (5.66)$$

in excellent agreement with the experimental value [53] $H = -2.68 \pm 0.68$. The next-to-leading order corrections to H have also been calculated [65]. If the new low-energy parameters are estimated using the vector mesons only, these corrections are small.

The results for F, G and R must satisfy two nontrivial constraints: i) Unitarity requires that F, G and R contain, in the physical region $4M_\pi^2 \leq s_\pi \leq (M_K - m_l)^2$, imaginary parts governed by S - and P -wave $\pi\pi$ scattering [these imaginary parts are contained in the functions $\Delta_0(s_\pi), \Delta_1(s_\pi)$]. ii) The scale dependence of the low-energy constants L_i^r must be compensated by the scale dependence of $U_{F,G,Z,Q}$ and $C_{F,G,Z,Q}$ for all values of $s_\pi, t, u, M_\pi^2, M_K^2$. [Since we work at order E^4 in the chiral expansion, the meson masses appearing in the above expressions satisfy the Gell-Mann-Okubo mass formula.] We have checked that these constraints are satisfied.

Because the one-loop contributions are rather large, one expects still substantial corrections from higher orders. In the following section, we therefore first estimate the effects from higher orders in the chiral expansion, using then this improved representation for the form factors in a comparison with the data.

5.7.3 Form factors beyond one loop

To investigate the importance of higher-order terms, we employ the method developed in Ref. [66]. It amounts to writing a dispersive representation of the partial wave amplitudes, fixing the subtraction constants using chiral perturbation theory. Here, we estimate the higher-order terms in the S -wave projection of the amplitude F_1 ,

$$f(s_\pi, s_l) = (4\pi X)^{-1} \int d\Omega F_1(s_\pi, t, s_l) , \quad (5.67)$$

because this form factor plays a decisive role in the determination of L_1^r, L_2^r and L_3 , and it is influenced by S -wave $\pi\pi$ scattering which is known [67] to produce substantial corrections.

5.7.4 Analytic properties of partial waves

Only the crossing-even part

$$F_1^+ = XF^+ + \sigma_\pi(PL) \cos \theta_\pi \cdot G^- \quad (5.68)$$

contributes in the projection (5.67). The partial wave f has the following analytic properties:

1. At fixed s_l , it is analytic in the complex s_π -plane, cut along the real axis for $\text{Re } s_\pi \geq 4M_\pi^2$ and $\text{Re } s_\pi \leq 0$.
2. In the interval $0 \leq s_\pi \leq 4M_\pi^2$, it is real.
3. In $4M_\pi^2 \leq s_\pi \leq 16M_\pi^2$, its phase coincides with the isospin zero S -wave phase δ_0^0 in elastic $\pi\pi$ scattering,

$$f_+ = e^{2i\delta_0^0} f_- , f_\pm = f(s_\pi \pm i\epsilon, s_l). \quad (5.69)$$

The proof of these properties is standard [68]. Here we only note that the presence of the cut for $s_\pi \leq 0$ follows from the relations

$$\begin{aligned} t &= M_\pi^2 + \frac{M_K^2 + s_l - s_\pi}{2} - \sigma_\pi X \cos \theta_\pi , \\ t(\cos \theta_\pi = -1, s_\pi < 0) &\geq (M_K + M_\pi)^2. \end{aligned} \quad (5.70)$$

Since F^+ and G^- have cuts at $t \geq (M_K + M_\pi)^2$, the claim is proven.

5.7.5 Unitarization

We introduce the Omnès function

$$\Omega(s_\pi) = \exp \left[\frac{s_\pi}{\pi} \int_{4M_\pi^2}^{\Lambda^2} \frac{ds}{s} \frac{\delta_0^0(s)}{s - s_\pi} \right] , \quad (5.71)$$

where Λ will be chosen of the order of 1 GeV below. According to (5.69), multiplication by Ω^{-1} removes the cut in f for $4M_\pi^2 \leq s_\pi \leq 16M_\pi^2$. Consider now

$$f = f_L + f_R , \quad (5.72)$$

where $f_L(f_R)$ has only the left-hand (right-hand) cut, and introduce

$$v = \Omega^{-1}(f - f_L) . \quad (5.73)$$

Then v has only a right-hand cut, and we may represent it in a dispersive way,

$$v = v_0 + v_1 s_\pi + \frac{s_\pi^2}{\pi} \int_{4M_\pi^2}^{\infty} \frac{ds}{s^2} \frac{\text{Im}\Omega^{-1}(f - f_L)}{s - s_\pi} . \quad (5.74)$$

We expect the contributions from the integral beyond 1 GeV² to be small. Furthermore, $\Omega^{-1}f$ is approximately real between $16M_\pi^2$ and 1 GeV², as a result of which one has

$$v = v_0 + v_1 s_\pi - \frac{s_\pi^2}{\pi} \int_{4M_\pi^2}^{\Lambda^2} \frac{ds}{s^2} \frac{f_L \text{Im}\Omega^{-1}}{s - s_\pi} . \quad (5.75)$$

For given v_0, v_1, f_L and Ω , the form factor f is finally obtained from

$$f = f_L + \Omega v . \quad (5.76)$$

The behaviour of f_L at $s_\pi \rightarrow 0$ is governed by the large- $|t|$ behaviour of F^+ and G^- , see (5.70). Therefore, instead of using CHPT to model f_L , we approximate the left-hand cut by resonance exchange. To pin down the subtraction constants v_0 and v_1 , we require that the threshold expansion of f and f_{CHPT} agree up to and including terms of order $O(E^2)$. For a specific choice of f_L , this fixes v_0, v_1 in terms of the quantities which occur in the one-loop representation of F^+ and G^- . In the case where $f_L = 0$, f has then a particularly simple form at $s_l = 0$,

$$\begin{aligned} f(s_\pi, s_l = 0)|_{f_L=0} &= \Omega(v_0 + v_1 s_\pi) , \\ v_0 &= \frac{M_K}{\sqrt{2}F_\pi} \left\{ 1.05 + \frac{1}{F_\pi^2} \left[-64M_\pi^2 L_1^r + 8M_K^2 L_2^r \right. \right. \\ &\quad \left. \left. + 2(M_K^2 - 8M_\pi^2)L_3 + \frac{2}{3}(M_K^2 - 4M_\pi^2)(4L_2^r + L_3) \right] \right\} , \\ v_1 &= \frac{M_K}{\sqrt{2}F_\pi} \left\{ 0.38 + \frac{1}{F_\pi^2} \left[32L_1^r + 8L_2^r + 10L_3 \right. \right. \\ &\quad \left. \left. - \frac{2}{3} \frac{M_K^2 - 4M_\pi^2}{4M_\pi^2} (4L_2^r + L_3) \right] \right\} . \end{aligned} \quad (5.77)$$

The details of the evaluation of f_L, v_0 and of v_1 may be found in Ref. [62].

In the partial wave f , the effects of the final-state interactions are substantial, because they are related to the $I = 0, S$ -wave $\pi\pi$ phase shift. On the other hand, for the leading partial wave in $G^+ = ge^{i\delta_p} + \dots$, these effects are reduced, because the phase δ_p is small at low energies. We find it more difficult to assess an estimate for the higher-order corrections in this case – we come back to this point in the following sections.

We add a remark concerning the choice of the subtraction point in the Omnès function (5.71). To remove the right-hand cut in f , the modified Omnès function

$$\Omega(s_\pi, s_0) = \exp \frac{(s_\pi - s_0)}{\pi} \int_{4M_\pi^2}^{\Lambda^2} \frac{ds}{s - s_0} \frac{\delta_0^0(s)}{s - s_\pi}$$

would do as well, with any value of $s_0 \leq 4M_\pi^2$. To illustrate the meaning of s_0 , we consider for simplicity the form factor f in the case where $f_L = 0$. The choice $s_0 = 4M_\pi^2$ then amounts to the statement that, at threshold, there are no contributions from two loops and beyond by fiat. We consider this to be rather unlikely. (For a different opinion see [69].) On the other hand, we have checked that our results do not vary significantly if s_0 is taken of the order of the pion mass squared, $|s_0| \leq M_\pi^2$.

5.8 Determination of L_1, L_2 and L_3

To illustrate the usefulness of forthcoming more accurate K_{l4} data, we determine here the low-energy constants L_1^r, L_2^r and L_3 from data on $K^+ \rightarrow \pi^+ \pi^- e^+ \nu_e$ decays and on $\pi\pi \rightarrow \pi\pi$ threshold parameters, using the improved S -wave amplitude f set up above. For a comparison with earlier work [55] we refer the reader to Ref. [62].

We perform fits to $f_s(0), \lambda_f, g(0)$ as given in (5.37) and to the $\pi\pi$ threshold parameters listed in table 5.2. We introduce for this purpose the quantities

$$\begin{aligned}\bar{f}(s_\pi, s_l) &= \left| (4\pi X)^{-1} \int d\Omega F_1(s_\pi, t, s_l) \right| = |f(s_\pi, s_l)| \quad , \\ \bar{g}(s_\pi, s_l) &= \left| \frac{3}{8\pi} \int d\Omega \sin^2 \theta_\pi G(s_\pi, t, s_l) \right| \quad ,\end{aligned}\tag{5.78}$$

where the factor $3/2 \sin^2 \theta$ appears because G is expanded in derivatives of Legendre polynomials. Below, we identify $[f_s(0), g(0)]$ with $[\bar{f}(4M_\pi^2, s_l), \bar{g}(4M_\pi^2, s_l)]$, which depend on s_l . Furthermore, we compare the slope λ_f with

$$\bar{\lambda}_f(s_\pi, s_l) = \frac{\bar{f}(s_\pi, s_l) - \bar{f}(4M_\pi^2, s_l)}{\bar{f}(4M_\pi^2, s_l)} \frac{4M_\pi^2}{s_\pi - 4M_\pi^2} \quad ,\tag{5.79}$$

which depends on both s_π and s_l . We use these dependences to estimate systematic uncertainties in the determination of the low-energy couplings. [In future high-statistics experiments, the s_l -dependence of the form factors will presumably be resolved. It will be easy to adapt the procedure to this case.]

We have used MINUIT [70] to perform the fits. The results for the choice $s_l = 0, s_\pi = 4.4M_\pi^2$ are given in table 5.2. In the columns denoted by “one-loop”, we have evaluated \bar{f}, \bar{g} and $\bar{\lambda}_f$ from the one-loop representation given above⁹. In the fit with the unitarized form factor (columns 3 and 5), we have evaluated \bar{f} from Eqs. (5.76), inserting in the Omnès function the parametrization of the $\pi\pi$ S -wave phase shift proposed by Schenk [72, solution B]. For the form factor G , we have again used the one-loop representation. The statistical errors quoted for the L_i ’s are the ones generated by the procedure MINOS in MINUIT and correspond to an increase of χ^2 by one unit.

A few remarks are in order at this place.

⁹We always use for L_4^r, \dots, L_9^r the values quoted in table 1 of Ref. [2].

Table 5.2: Results of fits with one-loop and unitarized form factors, respectively. The errors quoted for the L_i^r 's are statistical only. The L_i^r are given in units of 10^{-3} at the scale $\mu = M_\rho$, the scattering lengths a_i^I and the slopes b_i^I in appropriate powers of M_{π^+} .

	K_{e4} data alone		K_{e4} and $\pi\pi$ data		experiment
	one-loop	unitarized	one-loop	unitarized	[71]
L_1^r	0.65 ± 0.27	0.36 ± 0.26	0.60 ± 0.24	0.37 ± 0.23	
L_2^r	1.63 ± 0.28	1.35 ± 0.27	1.50 ± 0.23	1.35 ± 0.23	
L_3	-3.4 ± 1.0	-3.4 ± 1.0	-3.3 ± 0.86	-3.5 ± 0.85	
a_0^0	0.20	0.20	0.20	0.20	0.26 ± 0.05
b_0^0	0.26	0.25	0.26	0.25	0.25 ± 0.03
$-10 a_0^2$	0.40	0.41	0.40	0.41	0.28 ± 0.12
$-10 b_0^2$	0.67	0.72	0.68	0.72	0.82 ± 0.08
$10 a_1^1$	0.36	0.37	0.36	0.37	0.38 ± 0.02
$10^2 b_1^1$	0.44	0.47	0.43	0.48	
$10^2 a_2^0$	0.22	0.18	0.21	0.18	0.17 ± 0.03
$10^3 a_2^2$	0.39	0.21	0.37	0.20	0.13 ± 0.3
χ^2/N_{DOF}	0/0	0/0	8.8/7	4.9/7	

1. It is seen that the overall description of the $\pi\pi$ scattering data is better using the unitarized form factors, in particular so for the D -wave scattering lengths.
2. The errors quoted do not give account of the fact that the simultaneous determination of the three constants produces a strong correlation between them. To illustrate this point we note that, while the values of the L_i 's in column 4 and 5 are apparently consistent with each other within one error bar, the χ^2 in column 5 increases from 4.9 to 30.7 if the L_i 's from column 4 are used in the evaluation of χ^2 in column 5. (For a discussion about the interpretation of the errors see [70]).
3. The low-energy constants \bar{l}_1, \bar{l}_2 which occur in $SU(2)_L \times SU(2)_R$ analyses may be evaluated from a given set of L_1^r, L_2^r and L_3 [44]. Their value changes in a significant way by using the unitarized amplitude instead of the one-loop formulae: the values for (\bar{l}_1, \bar{l}_2) in column 4 and 5 are $(-0.5 \pm 0.88, 6.4 \pm 0.44)$ and $(-1.7 \pm 0.85, 6.0 \pm 0.4)$, respectively.
4. L_1^r, L_2^r and L_3 are related to $\pi\pi$ phase shifts through sum rules [73, 74]. In principle, one could take these constraints into account as well¹⁰. We do not consider them here, because we find it very difficult to assess a reliable error for the integrals over the total $\pi\pi$ cross sections which occur in those relations.

¹⁰We thank B. Moussallam for pointing this out to us.

The *statistical* error in the data is only one source of the uncertainty in the low-energy constants, which are in addition affected by the ambiguities in the estimate of the higher-order corrections. These *systematic* uncertainties have several sources:

- i) Higher-order corrections to \bar{g} have not been taken into account.
- ii) The determination of the contribution from the left-hand cut is not unique.
- iii) The quantities \bar{f} and \bar{g} depend on s_l , and $\bar{\lambda}_f$ is a function of both s_l and s_π .
- iv) The Omnès function depends on the elastic $\pi\pi$ phase shift and on the cutoff Λ used.

We have considered carefully these effects [62], and found that the best determination of L_1^r, L_2^r , and L_3 which takes them into account is

$$\begin{aligned} 10^3 L_1^r(M_\rho) &= 0.4 \pm 0.3 , \\ 10^3 L_2^r(M_\rho) &= 1.35 \pm 0.3 , \\ 10^3 L_3 &= -3.5 \pm 1.1 . \end{aligned} \tag{5.80}$$

These values are the ones quoted in table 1 in Ref. [2]. For $SU(2)_L \times SU(2)_R$ analyses it is useful to know the corresponding values for the constants \bar{l}_1 and \bar{l}_2 ,

$$\begin{aligned} \bar{l}_1 &= -1.7 \pm 1.0 , \\ \bar{l}_2 &= 6.1 \pm 0.5 . \end{aligned} \tag{5.81}$$

The value and uncertainties in these couplings play a decisive role in a planned experiment [75] to measure the lifetime of $\pi^+\pi^-$ atoms, which will provide a completely independent measurement of the $\pi\pi$ scattering lengths $|a_0^0 - a_0^2|$.

One motivation for the analysis in [54, 55] was to test the large- N_C prediction $L_2^r = 2L_1^r$. The above result shows that a small non-zero value is preferred. To obtain a clean error analysis, we have repeated the fitting procedure using the variables

$$\begin{aligned} X_1 &= L_2^r - 2L_1^r - L_3 , \\ X_2^r &= L_2^r , \\ X_3 &= (L_2^r - 2L_1^r)/L_3 . \end{aligned} \tag{5.82}$$

We performed a fit to K_{e4} and $\pi\pi$ data, including the theoretical error in G as discussed above, and found

$$\begin{aligned} X_1 &= (4.8 \pm 0.8) \cdot 10^{-3} , \\ X_3 &= -0.17_{-0.22}^{+0.12} . \end{aligned} \tag{5.83}$$

The result is that the large- N_C prediction works remarkably well.

Table 5.3: Approximations used to evaluate the total rates in table 5.4. Use of $\bar{f} = \bar{f}_{\text{CHPT}}$, $\bar{g} = \bar{g}_{\text{CHPT}}$ reproduces the one-loop results in table 5.4 to about 1%.

a) K^+ decays

	$\pi^0 \pi^0 e^+ \nu_e$	$\pi^+ \pi^- \mu^+ \nu_\mu$	$\pi^0 \pi^0 \mu^+ \nu_\mu$
F_1	$-X\bar{f}$	$X\bar{f} + \sigma_\pi(PL) \cos \theta_\pi \bar{g}$	$-X\bar{f}$
F_2	0	$\sigma_\pi(s_\pi s_l)^{1/2} \bar{g}$	0
F_3	0	0	0
F_4	$(PL)\bar{f}$	$-\{(PL)\bar{f} + s_l R_{\text{CHPT}} + \sigma_\pi X \cos \theta_\pi \bar{g}\}$	$\{(PL)\bar{f} + s_l R_{\text{CHPT}}^+\}$

b) K^0 decays. Shown are the amplitudes divided by $\sqrt{2}$.

	$\pi^0 \pi^- e^+ \nu_e$	$\pi^0 \pi^- \mu^+ \nu_\mu$
F_1	$X F_{\text{CHPT}}^- + \sigma_\pi(PL) \cos \theta_\pi \bar{g}$	$X F_{\text{CHPT}}^- + \sigma_\pi(PL) \cos \theta_\pi \bar{g}$
F_2	$\sigma_\pi(s_\pi s_l)^{1/2} \bar{g}$	$\sigma_\pi(s_\pi s_l)^{1/2} \bar{g}$
F_3	0	0
F_4	$-\{(PL)F_{\text{CHPT}}^- + \sigma_\pi X \cos \theta_\pi \bar{g}\}$	$-\{(PL)F_{\text{CHPT}}^- + s_l R_{\text{CHPT}}^- + \sigma_\pi X \cos \theta_\pi \bar{g}\}$

5.9 Predictions

In this section we make several predictions using the L_i^r 's from table 1 in Ref. [2]. It is clear that new and more accurate data on K_{e4} will allow for a better determination of L_1^r, L_2^r and L_3 , and may correspondingly modify our predictions. However, unless a dramatic change in the values of these constants occurs, the modified predictions will be within the errors that we give.

Whereas the slope λ_g was assumed to coincide with the slope λ_f in the final analysis of the data in Ref. [53], these two quantities may differ in the chiral representation. Furthermore, our amplitudes allow us to evaluate partial and total decay rates. In this section, we consider the slope λ_g and the total rates.

The slope λ_g

We consider the form factor \bar{g} introduced in (5.78) and determine its slope λ_g

$$\bar{g}(s_\pi, s_l) = \bar{g}(4M_\pi^2, s_l)(1 + \lambda_g(s_l)q^2 + O(q^4)) \quad (5.84)$$

Table 5.4: Total decay rates in sec^{-1} . To evaluate the rates at one-loop accuracy, we have used the L_i^r 's from table 1 in Ref. [2]. The final predictions are evaluated with the amplitudes shown in table 5.3, using $\bar{f} = 5.59(1 + 0.08q^2)$, $\bar{g} = 4.77(1 + 0.08q^2)$. For the evaluation of the uncertainties in the rates see text.

a) K^+ decays

	$\pi^+\pi^-e^+\nu_e$	$\pi^0\pi^0e^+\nu_e$	$\pi^+\pi^-\mu^+\nu_\mu$	$\pi^0\pi^0\mu^+\nu_\mu$
tree	1297	683	155	102
one-loop	2447	1301	288	189
final	input	1625	333	225
prediction		± 90	± 15	± 11
experiment	3160	1700	1130	
[3]	± 140	± 320	± 730	

b) K^0 decays

	$\pi^0\pi^-e^+\nu_e$	$\pi^0\pi^-\mu^+\nu_\mu$
tree	561	55
one-loop	953	94
final	917	88
prediction	± 170	± 22
experiment	998	
[60]	$\pm 39 \pm 43$	

from the one-loop expression for G . The result is $\lambda_g(0) = 0.08$. As the slope is a one-loop effect, higher-order corrections may affect its value substantially. For this reason, we have evaluated λ_g also from the modified form factor obtained by using the complete resonance propagators (and the corresponding L_i 's), see Ref. [62]. The change is $\Delta\lambda_g = 0.025$. We believe this to be a generous error estimate and obtain in this manner

$$\lambda_g(0) = 0.08 \pm 0.025 \quad . \quad (5.85)$$

The central value indeed agrees with the slope λ in (5.37).

Total rates

Once the leading partial waves \bar{f} and \bar{g} are known from e.g. $K^+ \rightarrow \pi^+\pi^-e^+\nu_e$ decays, the chiral representation allows one to predict the remaining rates within rather small

uncertainties. We illustrate the procedure for $K^+ \rightarrow \pi^0 \pi^0 e^+ \nu_e$. According to Eq. (5.24), the relevant amplitude is determined by F^+, G^-, R^+ and H^- . The contribution from H is kinematically strongly suppressed and completely negligible in all total rates, whereas the contribution from R is negligible in the electron modes. Using the chiral representation of the amplitudes F^+ and G^- , we find that the rate is reproduced to about 1%, if one neglects G^- altogether and uses only the leading partial wave in the remaining amplitude, $F_1^+ \simeq -X\bar{f}$. From the measured [53] form factor $\bar{f} = 5.59(1 + 0.08q^2)$ we then find $\Gamma_{K^+ \rightarrow \pi^0 \pi^0 e^+ \nu_e} = 1625 \text{sec}^{-1}$. Finally, we estimate the error from

$$\begin{aligned} \Delta\Gamma = & \left\{ [\Gamma(f_s(0) + \Delta f_s, \lambda_f) - \Gamma(f_s(0), \lambda_f)]^2 + \right. \\ & \left. [\Gamma(f_s(0), \lambda_f + \Delta\lambda_f) - \Gamma(f_s(0), \lambda_f)]^2 \right\}^{1/2} = 90 \text{sec}^{-1} , \end{aligned} \quad (5.86)$$

where $\Delta f_s = 0.14, \Delta\lambda_f = 0.02$. The final result for the rate is shown in the row “final prediction” in table 5.4, where we have also listed the tree and the one-loop result, together with the experimental data. The evaluation of the remaining rates is done in a similar manner – see table 5.3 for the simplifications used and table 5.4 for the corresponding predictions.

We have assessed an uncertainty due to contributions from $F_{\text{CHPT}}^-, R_{\text{CHPT}}$ in the following manner. i) We have checked that the results barely change by using the tree level expression for R_{CHPT} instead of its one-loop representation. We conclude from this that the uncertainties in R_{CHPT} do not matter. ii) The uncertainty from F_{CHPT}^- is taken into account by adding to $\Delta\Gamma$ in quadrature the change obtained by evaluating F_{CHPT}^- at $L_3 = -3.5 + 1.1 = -2.4$. iii) In K^0 decays, we have also added in quadrature the difference generated by evaluating the rate with $M_\pi = 135 \text{ MeV}$.

The decay $K^0 \rightarrow \pi^0 \pi^- e^+ \nu_e$ has recently been measured [60] with considerably higher statistics than before [3]. We display the result for the rate in the first column of table 5.4b. The quoted errors correspond to the errors in the branching ratio [60] and do not include the uncertainty in the total decay rate quoted by the PDG [3]. Notice that the value for L_3 determined in [60] should be multiplied with -1 [76].

5.10 Improvements at DAΦNE

The chiral analysis of K_{l4} decays has been used so far for three purposes:

1. The K_{e4} data from Ref. [53] allows one to make predictions for the slope of the G form factor, for the total rates in all the channels and for the $\pi\pi$ scattering lengths. These are given in Eq. (5.85), in table 5.4 and in table 5.2, respectively.
2. The same K_{e4} data allow one to test the large- N_C prediction, see Eqs. (5.82) and (5.83).

3. The full set of K_{e4} and $\pi\pi$ scattering data allows the best determination of the coefficients L_1, L_2 and L_3 in the chiral Lagrangian, see (5.80).

In the next generation of K_{l4} decay experiments, there is the opportunity to improve the phenomenology of K_{l4} (see table 5.1):

1. A very useful innovation would be to analyze the experimental data with a modified chiral representation. In the latter, the full S - and P - wave parts of F_1 and F_2 could be inserted, using the chiral representation solely to describe the small background effects due to higher partial waves $l \geq 2$. To be more precise, one would take for R and H the one-loop chiral representation, whereas for G one writes

$$\begin{aligned} G &= g(s_\pi, s_l) e^{i\delta_p} + \Delta G, \\ \Delta G &= G_{\text{CHPT}} - \frac{3}{8\pi} \int d\Omega \sin^2 \theta_\pi G_{\text{CHPT}}, \end{aligned} \quad (5.87)$$

and similarly for F . The unknown amplitudes $g(s_\pi, s_l), f_s(s_\pi, s_l)$ and the phases δ_p, δ_s would then be determined from the data. We have checked that, if the errors in the form factors determined in this manner can be reduced by e.g. a factor 3 with respect to the ones shown in (5.37), one could pin down particular combinations of L_1^r, L_2^r and L_3 to considerably better precision than was shown above. This is true independently of an eventual improvement in the theoretical determination of the higher-order corrections in the form factor G – which is a theoretical challenge in any case.

2. The present experimental uncertainty on G is still too large to provide a precise value for the large- N_C parameter $(L_2^r - 2L_1^r)/L_3$. ($K^0 \rightarrow \pi^0 \pi^- e^+ \nu_e$ decays are mainly sensitive to G_{+-}^+ which in turn can be used to pin down L_3 . $K^+ \rightarrow \pi^0 \pi^0 e^+ \nu_e$ is mainly sensitive to F_{+-}^+ which contains L_1, L_2 and L_3 .)
3. The observation of all K_{l4} reactions with high statistics could provide a cleaner separation of the various isospin amplitudes.
4. Finally, we come to a most important point. As we mentioned already, $K^+ \rightarrow \pi^+ \pi^- e^+ \nu_e$ has been used [59] to determine the isoscalar S -wave scattering length with the result $a_0^0 = 0.26 \pm 0.05$. This value must be compared with the $\text{SU}(2) \times \text{SU}(2)$ prediction [77, 78] $a_0^0 = 0.20 \pm 0.01$. Low-energy $\pi\pi$ scattering is one of the few places where chiral symmetry allows one to make a precise prediction within the framework of QCD. In their article, Rosselet et al. comment about the discrepancy between $a_0^0 = 0.26 \pm 0.05$ and the leading-order result [79] $a_0^0 = 0.16$ in the following manner: “... it appears that this prediction can be revised without any fundamental change in current algebra or in the partial conservation of axial-vector current [80, 81].” Today, we know that this is not the case: The standard picture of the vacuum structure in QCD [82] would have to be revised, should the central value $a_0^0 = 0.26$ be confirmed

with a substantially smaller error. For recent work which supports this scenario see the contribution of Knecht and Stern in this Handbook [83].

K_{l4} decays are – at present [75] – the only available source of clean information on $\pi\pi$ S -wave scattering near threshold. We refer the reader to Ref. [84] for a detailed analysis of the issue.

6 K_{e5} decays

In this subsection we discuss ¹¹ the decays

$$\begin{aligned} K^+ &\rightarrow \pi^+\pi^-\pi^0 e^+\nu_e \\ K^+ &\rightarrow \pi^0\pi^0\pi^0 e^+\nu_e \\ K^0 &\rightarrow \pi^0\pi^0\pi^-\pi^+ e^+\nu_e \\ K^0 &\rightarrow \pi^+\pi^-\pi^-\pi^+ e^+\nu_e . \end{aligned} \quad (6.1)$$

We do not consider isospin violating contributions and correspondingly set $m_u = m_d$, $\alpha = 0$.

6.1 Matrix elements and decay rates

The matrix element for $K \rightarrow \pi\pi\pi e^+\nu_e$ is

$$T = \frac{G_F}{\sqrt{2}} V_{us}^* \bar{u}(p_\nu) \gamma_\mu (1 - \gamma_5) v(p_e) (V^\mu - A^\mu) , \quad (6.2)$$

where

$$I_\mu = \langle \pi(p_1)\pi(p_2)\pi(p_3)_{\text{out}} | I_\mu^{4-i5}(0) | K(p) \rangle ; \quad I = V, A. \quad (6.3)$$

The decay rate is calculated from

$$d\Gamma = \frac{1}{2M_K(2\pi)^{11}} \sum_{\text{spins}} |T|^2 d_{LIPS}(p; p_e, p_\nu, p_1, p_2, p_3) .$$

6.2 Previous experiments

The Particle Data Group [3] quotes the upper bound

$$BR(K^+ \rightarrow \pi^0\pi^0\pi^0 e^+\nu_e) < 3.5 \cdot 10^{-6}.$$

¹¹The material in this section is taken from Ref. [85].

Table 6.1: Rates of K_{e5} decays, evaluated from the leading-order term.

	branching ratio
$K^+ \rightarrow \pi^+ \pi^- \pi^0 e^+ \nu_e$	$3 \cdot 10^{-12}$
$K^+ \rightarrow \pi^0 \pi^0 \pi^0 e^+ \nu_e$	$2.5 \cdot 10^{-12}$
$K^0 \rightarrow \pi^0 \pi^0 \pi^- e^+ \nu_e$	$12 \cdot 10^{-12}$
$K^0 \rightarrow \pi^+ \pi^- \pi^- e^+ \nu_e$	$33 \cdot 10^{-12}$

6.3 Theory

In CHPT, the leading-order contribution is given by the matrix element of the *vector* current. The corresponding rates are displayed in table (6.1). The smallness of these rates is due to the suppression of phase space. Indeed, consider the ratio of the four- and five-dimensional phase space volumes in the neutral pion channel,

$$\frac{M_K^2 \int d_{LISP}(p; p_e, p_\nu, p_1, p_2)/2!}{(2\pi)^{12}} \frac{(2\pi)^{15}}{\int d_{LISP}(p; p_e, p_\nu, p_1, p_2, p_3)/3!} \simeq 2.3 \cdot 10^6 \quad .$$

It agrees well with the ratio of the corresponding rates at tree level,

$$\frac{\Gamma(K^+ \rightarrow \pi^0 \pi^0 e^+ \nu_e)_{tree}}{\Gamma(K^+ \rightarrow \pi^0 \pi^0 \pi^0 e^+ \nu_e)_{tree}} \simeq 3.4 \cdot 10^6 \quad .$$

(The corresponding ratios for $K^+ \rightarrow \pi^0 e^+ \nu_e / K^+ \rightarrow \pi^0 \pi^0 e^+ \nu_e$ are $1.4 \cdot 10^4$ and $0.53 \cdot 10^4$ for phase space volumes and decay rates, respectively.) The contributions at order p^4 are due to i) the corrections to the matrix element of the vector current, and to ii) the matrix element of the *axial* current. The latter stems from the Wess-Zumino-Witten Lagrangian \mathcal{L}_{WZW} . Both the local and nonlocal term in the anomalous action contribute. The nonlocal part is suppressed by the factor m_e in the matrix element (in addition to the phase space suppression just mentioned).

Based on our experience with K_{e4} decays, we expect the terms of order p^4 to enhance the above rates by roughly a factor of two to three.

6.4 Improvements at DAΦNE

According to the standard model, K_{e5} decays are invisible at DAΦNE, but the existing upper limits can be improved significantly.

A Notation

The notation for phase space is the one without the factors of 2π . For the decay rate of a particle with four momentum p into n particles with momenta p_1, \dots, p_n this is

$$d_{LIPS}(p; p_1, \dots, p_n) = \delta^4(p - \sum_{i=1}^n p_i) \prod_{i=1}^n \frac{d^3 p_i}{2p_i^0} . \quad (\text{A.1})$$

We use a covariant normalization of one-particle states,

$$\langle \vec{p}' | \vec{p} \rangle = (2\pi)^3 2p^0 \delta^3(\vec{p}' - \vec{p}) , \quad (\text{A.2})$$

together with the spinor normalization

$$\bar{u}(p, r) u(p, s) = 2m \delta_{rs} . \quad (\text{A.3})$$

The kinematical function $\lambda(x, y, z)$ is defined as

$$\lambda(x, y, z) = x^2 + y^2 + z^2 - 2(xy + yz + zx) . \quad (\text{A.4})$$

We take the standard model in the current \times current form, i.e., we neglect the momentum dependence of the W -propagator. The currents used in the text are :

$$\begin{aligned} V_\mu^{4-i5} &= \bar{q} \gamma_\mu \frac{1}{2} (\lambda_4 - i\lambda_5) q = \bar{s} \gamma_\mu u \\ A_\mu^{4-i5} &= \bar{q} \gamma_\mu \gamma_5 \frac{1}{2} (\lambda_4 - i\lambda_5) q = \bar{s} \gamma_\mu \gamma_5 u \\ V_\mu^{em} &= \bar{q} \gamma_\mu Q q \\ Q &= \text{diag}(2/3, -1/3, -1/3) . \end{aligned} \quad (\text{A.5})$$

The numerical values used in the programs are the physical masses for the particles as given by the Particle Data Group [3]. In addition we have used the values for the decay constants derived from the most recent measured charged pion and kaon semileptonic decay rates[3, 26] :

$$\begin{aligned} F_\pi &= 93.2 \text{ MeV} \\ F_K &= 113.6 \text{ MeV} . \end{aligned} \quad (\text{A.6})$$

We do not need values for the quark masses. For the processes considered in this report we can always use the lowest order relations to rewrite them in terms of the pseudoscalar meson masses (see Ref. [2]). For the KM matrix element we used the central value $|V_{us}| = 0.220$ of Ref. [3]. The numerical values for the $L_i^r(M_\rho)$ are those given in table 1 in Ref. [2].

The number of events quoted for DAΦNE are based on a luminosity of $5 \cdot 10^{32} \text{ cm}^{-2} \text{ s}^{-1}$, which is equivalent [1] to an annual rate of $9 \cdot 10^9$ ($1.1 \cdot 10^9$) tagged K^\pm (K_L) (1 year = 10^7 s assumed).

Whenever we quote a branching ratio for a semileptonic K^0 decay, it stands for the branching ratio of the corresponding K_L decay, e.g.,

$$BR(K^0 \rightarrow \pi^- l^+ \nu) \equiv BR(K_L \rightarrow \pi^\pm l^\mp \nu) . \quad (\text{A.7})$$

We use the Condon-Shortley phase conventions throughout.

B Loop integrals

In this appendix we define the functions appearing in the loop integrals used in the text. First we define the functions needed for loops with two propagators, mainly in the form given in Ref. [44]. We consider a loop with two masses, M and m . All needed functions can be given in terms of the subtracted scalar integral $\bar{J}(t) = J(t) - J(0)$,

$$J(t) = -i \int \frac{d^d p}{(2\pi)^d} \frac{1}{((p+k)^2 - M^2)(p^2 - m^2)} \quad (\text{B.1})$$

with $t = k^2$. The functions used in the text are then :

$$\begin{aligned} \bar{J}(t) &= -\frac{1}{16\pi^2} \int_0^1 dx \log \frac{M^2 - tx(1-x) - \Delta x}{M^2 - \Delta x} \\ &= \frac{1}{32\pi^2} \left\{ 2 + \frac{\Delta}{t} \log \frac{m^2}{M^2} - \frac{\Sigma}{\Delta} \log \frac{m^2}{M^2} - \frac{\sqrt{\lambda}}{t} \log \frac{(t + \sqrt{\lambda})^2 - \Delta^2}{(t - \sqrt{\lambda})^2 - \Delta^2} \right\} , \\ J^r(t) &= \bar{J}(t) - 2k , \\ M^r(t) &= \frac{1}{12t} \{t - 2\Sigma\} \bar{J}(t) + \frac{\Delta^2}{3t^2} \bar{J}(t) + \frac{1}{288\pi^2} - \frac{k}{6} \\ &\quad - \frac{1}{96\pi^2 t} \left\{ \Sigma + 2 \frac{M^2 m^2}{\Delta} \log \frac{m^2}{M^2} \right\} , \\ L(t) &= \frac{\Delta^2}{4t} \bar{J}(t) , \\ K(t) &= \frac{\Delta}{2t} \bar{J}(t) , \\ H(t) &= \frac{2}{3} \frac{L_9^r}{F^2} t + \frac{1}{F^2} [t M^r(t) - L(t)] , \\ \Delta &= M^2 - m^2 , \\ \Sigma &= M^2 + m^2 , \\ \lambda &= \lambda(t, M^2, m^2) = (t + \Delta)^2 - 4t M^2 . \end{aligned} \quad (\text{B.2})$$

In the text these are used with subscripts,

$$\bar{J}_{ij}(t) = \bar{J}(t) \quad \text{with} \quad M = M_i, m = M_j \quad (\text{B.3})$$

and similarly for the other symbols. The subtraction point dependent part is contained in the constant k

$$k = \frac{1}{32\pi^2} \frac{M^2 \log \left(\frac{M^2}{\mu^2} \right) - m^2 \log \left(\frac{m^2}{\mu^2} \right)}{M^2 - m^2} , \quad (\text{B.4})$$

where μ is the subtraction scale.

In addition, in subsection 4 these functions and symbols appear in a summation over loops I with

$$\begin{aligned} J_I(t) &= \bar{J}(t) \quad \text{with} \quad M = M_I, m = m_I ; \\ \Sigma_I &= M_I^2 + m_I^2 \end{aligned} \quad (\text{B.5})$$

and again similarly for the others. There the combination B_2 appears as well :

$$\begin{aligned} B_2(t, M^2, m^2) &= B_2(t, m^2, M^2) \\ &= \frac{1}{288\pi^2} (3\Sigma - t) - \frac{\lambda(t, M^2, m^2)\bar{J}(t)}{12t} + \frac{t\Sigma - 8M^2m^2}{384\pi^2\Delta} \log \frac{M^2}{m^2} . \end{aligned}$$

The last formula to be defined is the three propagator loop integral function $C(t_1, t_2, M^2, m^2)$ where one of the three external momenta has zero mass and two of the propagators have the same mass M . Here $t_1 = (q_1 + q_2)^2$, $t_2 = q_2^2$ and $q_1^2 = 0$.

$$\begin{aligned} C(t_1, t_2, M^2, m^2) &= -i \int \frac{d^4p}{(2\pi)^d} \frac{1}{(p^2 - M^2)((p + q_1)^2 - M^2)((p + q_1 + q_2)^2 - m^2)} \\ &= -\frac{1}{16\pi^2} \int_0^1 dx \int_0^{1-x} dy \frac{1}{M^2 - y(\Delta + t_1) + xy(t_1 - t_2) + y^2t_1} \\ &= \frac{1}{(4\pi)^2(t_1 - t_2)} \left\{ Li_2 \left(\frac{1}{y_+(t_2)} \right) + Li_2 \left(\frac{1}{y_-(t_2)} \right) \right. \\ &\quad \left. - Li_2 \left(\frac{1}{y_+(t_1)} \right) - Li_2 \left(\frac{1}{y_-(t_2)} \right) \right\} , \\ y_{\pm}(t) &= \frac{1}{2t} \left\{ t + \Delta \pm \sqrt{\lambda(t, M^2, m^2)} \right\} \end{aligned} \tag{B.6}$$

where Li_2 is the dilogarithm

$$Li_2(x) = - \int_0^1 \frac{dy}{y} \log(1 - xy) . \tag{B.7}$$

C Decomposition of the hadronic tensors $I^{\mu\nu}$

Here we consider the tensors

$$I^{\mu\nu} = \int dx e^{iqx + iWy} \langle 0 | TV_{em}^\mu(x) I_{4-i5}^\nu(y) | K^+(p) \rangle , \quad I = V, A \tag{C.1}$$

and detail their connection with the matrix element (1.2).

The general decomposition of $A^{\mu\nu}, V^{\mu\nu}$ in terms of Lorentz invariant amplitudes reads [9, 11] for $q^2 \neq 0$

$$\begin{aligned} \frac{1}{\sqrt{2}} A^{\mu\nu} &= -F_K \left\{ \frac{(2W^\mu + q^\mu)W^\nu}{M_K^2 - W^2} + g^{\mu\nu} \right\} \\ &+ A_1(qW g^{\mu\nu} - W^\mu q^\nu) + A_2(q^2 g^{\mu\nu} - q^\mu q^\nu) \\ &+ \left\{ \frac{2F_K(F_V^K(q^2) - 1)}{(M_K^2 - W^2)q^2} + A_3 \right\} (qW q^\mu - q^2 W^\mu) W^\nu \end{aligned} \tag{C.2}$$

and

$$\frac{1}{\sqrt{2}}V^{\mu\nu} = iV_1\epsilon^{\mu\nu\alpha\beta}q_\alpha p_\beta \quad (\text{C.3})$$

where the form factors $A_i(q^2, W^2)$ and $V_1(q^2, W^2)$ are analytic functions of q^2 and W^2 . $F_V^K(q^2)$ denotes the electromagnetic form factor of the kaon ($F_V^K(0) = 1$). $A^{\mu\nu}$ satisfies the Ward identity

$$q_\mu A^{\mu\nu} = -\sqrt{2}F_K p^\nu. \quad (\text{C.4})$$

In the process (1.1) the photon is real. As a consequence of this, only the two form factors $A_1(0, W^2)$ and $V_1(0, W^2)$ contribute. We set

$$\begin{aligned} A(W^2) &= A_1(0, W^2) \\ V(W^2) &= V_1(0, W^2) \end{aligned} \quad (\text{C.5})$$

and obtain for the matrix element (1.2)

$$T = -iG_F/\sqrt{2}eV_{us}^* \epsilon_\mu^* \left\{ \sqrt{2}F_K l_1^\mu - (V^{\mu\nu} - A^{\mu\nu})l_\nu \right\} \Big|_{q^2=0}, \quad (\text{C.6})$$

with

$$\begin{aligned} l^\mu &= \bar{u}(p_\nu)\gamma^\mu(1 - \gamma_5)v(p_l) \\ l_1^\mu &= l^\mu + m_l \bar{u}(p_\nu)(1 + \gamma_5) \frac{2p_l^\mu + \not{q}\gamma^\mu}{m_l^2 - (p_l + q)^2} v(p_l). \end{aligned} \quad (\text{C.7})$$

Grouping terms into an IB and a SD piece gives (1.2,1.3). As a consequence of (C.4), T is invariant under the gauge transformation $\epsilon_\mu \rightarrow \epsilon_\mu + q_\mu$.

The amplitudes A_1, A_2 and V_1 are related to the corresponding quantities F_A, R and F_V used by the PDG [3] by

$$-\sqrt{2}M_K(A_1, A_2, V_1) = (F_A, R, F_V). \quad (\text{C.8})$$

The last term in (C.2) is omitted in [3]. It contributes to processes with a virtual photon, $K^\pm \rightarrow l^\pm \nu_l l'^+ l'^-$.

Finally, the relation to the notation used in [4, 5] is

$$\begin{aligned} 2(A \pm V)^2 &= (a_k \pm v_k)^2 \quad [4] \\ \sqrt{2}(A, V) &= (F_A, F_V) \quad [5]. \end{aligned} \quad (\text{C.9})$$

D One-loop corrections to K_{l4} form factors

In this appendix we give the expression of the unitarity corrections to the form factors F , G , and R ([54],[55],[62]).

$$U_F(s_\pi, t, u) = \Delta_0(s_\pi) + A_F(t) + B(t, u), \quad (\text{D.1})$$

with

$$\begin{aligned}
\Delta_0(s_\pi) &= \frac{1}{2}(2s_\pi - M_\pi^2)J_{\pi\pi}^r(s_\pi) + \frac{3s_\pi}{4}J_{KK}^r(s_\pi) + \frac{M_\pi^2}{2}J_{\eta\eta}^r(s_\pi) , \\
A_F(t) &= \frac{1}{16} \left[(14M_K^2 + 14M_\pi^2 - 19t)J_{K\pi}^r(t) + (2M_K^2 + 2M_\pi^2 - 3t)J_{\eta K}^r(t) \right] \\
&+ \frac{1}{8} \left[(3M_K^2 - 7M_\pi^2 + 5t)K_{K\pi}(t) + (M_K^2 - 5M_\pi^2 + 3t)K_{\eta K}(t) \right] \\
&- \frac{1}{4} \left[9(L_{K\pi}(t) + L_{\eta K}(t)) + (3M_K^2 - 3M_\pi^2 - 9t)(M_{K\pi}^r(t) + M_{\eta K}^r(t)) \right] , \\
B(t, u) &= -\frac{1}{2}(M_K^2 + M_\pi^2 - t)J_{K\pi}^r(t) - (t \leftrightarrow u). \tag{D.2}
\end{aligned}$$

The loop integrals $J_{\pi\pi}^r(s_\pi), \dots$ which occur in these expressions are listed in appendix B. The functions J_{PQ}^r and M_{PQ}^r depend on the scale μ at which the loops are renormalized. The scale drops out in the expression for the full amplitude.

The imaginary part of $F_\pi^{-2}\Delta_0(s_\pi)$ contains the $I = 0$, S -wave $\pi\pi$ phase shift

$$\delta_0^0(s_\pi) = (32\pi F_\pi^2)^{-1}(2s_\pi - M_\pi^2)\sigma_\pi + O(E^4) , \tag{D.3}$$

as well as contributions from $K\bar{K}$ and $\eta\eta$ intermediate states. The functions $A_F(t)$ and $B(t, u)$ are real in the physical region.

$$U_G(s_\pi, t, u) = \Delta_1(s_\pi) + A_G(t) + B(t, u) , \tag{D.4}$$

with

$$\begin{aligned}
\Delta_1(s_\pi) &= 2s_\pi \left\{ M_{\pi\pi}^r(s_\pi) + \frac{1}{2}M_{KK}^r(s_\pi) \right\} , \\
A_G(t) &= \frac{1}{16} \left[(2M_K^2 + 2M_\pi^2 + 3t)J_{K\pi}^r(t) - (2M_K^2 + 2M_\pi^2 - 3t)J_{\eta K}^r(t) \right] \\
&+ \frac{1}{8} \left[(-3M_K^2 + 7M_\pi^2 - 5t)K_{K\pi}(t) + (-M_K^2 + 5M_\pi^2 - 3t)K_{\eta K}(t) \right] \\
&- \frac{3}{4} \left[L_{K\pi}(t) + L_{\eta K}(t) - (M_K^2 - M_\pi^2 + t)(M_{K\pi}^r(t) + M_{\eta K}^r(t)) \right] . \tag{D.5}
\end{aligned}$$

The imaginary part of $F_\pi^{-2}\Delta_1(s_\pi)$ contains the $I = 1$, P -wave phase shift

$$\delta_1^1(s_\pi) = (96\pi F_\pi^2)^{-1}s_\pi\sigma_\pi^3 + O(E^4) . \tag{D.6}$$

as well as contributions from $K\bar{K}$ intermediate states. The function A_G is real in the physical region.

The unitarity corrections U_Z, U_Q in the form factor R in (5.58) are

$$\begin{aligned}
U_Z &= s_\pi \Delta_0(s_\pi) + \nu \Delta_1(s_\pi) - \frac{4}{9} M_K^2 M_\pi^2 J_{\eta\eta}^r(s_\pi) \\
&+ \frac{1}{32} \left[11(s_\pi - \nu)^2 - 20\Sigma(s_\pi - \nu) + 12\Sigma^2 \right] J_{K\pi}^r(t) \\
&+ \frac{1}{96} \left[3(s_\pi - \nu) - 2\Sigma \right]^2 J_{\eta K}^r(t) \\
&+ \frac{1}{4} (s_\pi + \nu)^2 J_{K\pi}^r(u) \\
&+ \frac{1}{4} (M_K^2 - M_\pi^2) [5(s_\pi - \nu) - 6\Sigma] K_{K\pi}(t) \\
&+ \frac{1}{4} (M_K^2 - M_\pi^2) [3(s_\pi - \nu) - 2\Sigma] K_{\eta K}(t) \\
&+ \frac{3}{8} \left[2s_\pi(\nu + 4\Sigma) - 3s_\pi^2 + \nu^2 - 16M_\pi^2 M_K^2 \right] \left[M_{K\pi}^r(t) + M_{\eta K}^r(t) \right] \\
&- \frac{3}{4} (3s_\pi + \nu - 2\Sigma) (L_{\eta K}(t) + L_{K\pi}(t)) , \tag{D.7}
\end{aligned}$$

$$\begin{aligned}
U_Q &= \Delta_0(s_\pi) + \frac{M_K^2 - s_l}{32} \left\{ 11J_{K\pi}^r(t) + 8J_{K\pi}^r(u) + 3J_{\eta K}^r(t) \right\} \\
&- \frac{1}{8} (5(s_\pi - \nu) + 5(M_K^2 - s_l) - 6\Sigma) K_{K\pi}(t) \\
&- \frac{1}{8} (3(s_\pi - \nu) + 3(M_K^2 - s_l) - 2\Sigma) K_{\eta K}(t) \\
&- \frac{9}{4} (L_{\eta K}(t) + L_{K\pi}(t)) \\
&+ \frac{3}{8} (4(\nu + 2M_\pi^2) - 3(M_K^2 - s_l)) (M_{K\pi}^r(t) + M_{\eta K}^r(t)) , \tag{D.8}
\end{aligned}$$

with

$$\Sigma = M_K^2 + M_\pi^2 .$$

Acknowledgements

We thank G. Pancheri for the perfect organization of the DAΦNE Workshops and the INFN for the hospitality in Frascati. We have enjoyed numerous interesting discussions with the members of the working groups. We thank J. Beringer for checking traces in $K_{l2\gamma}$, M. Candusso for doing the contour plots and C. Riggenbach for providing us with numerical routines for K_{l4} . S. Blaser kindly allowed us to include his work [85] on K_{e5} decays.

References

- [1] P. Franzini, private communication.
- [2] J. Bijnens, G. Ecker and J. Gasser, Chiral perturbation theory, this report.
- [3] Particle Data Group, Phys. Lett. B239 (1990).
We use this compilation throughout. Please contact one of the authors in case that very high precision is needed for a particular matrix element. We would then convert the relevant quantity to the newest data compilation available.
- [4] J. Heintze et al., Nucl. Phys. B149 (1979) 365.
- [5] Y. Akiba et al., Phys. Rev. D32 (1985) 2911.
- [6] S.G. Brown and S.A. Bludman, Phys. Rev. B136 (1964) 1160;
D.A. Bryman et al., Phys. Rep. C88 (1982) 151.
- [7] K.S. Heard et al., Phys. Lett. 55B (1975) 324.
- [8] V.V. Barmin et al., Sov. J. Nucl. Phys. 47 (1988) 643.
- [9] D. Yu. Bardin and E. A. Ivanov, Sov. J. Part. Nucl. 7 (1976) 286.
- [10] J.F. Donoghue and B.R. Holstein, Phys. Rev. D40 (1989) 3700.
- [11] J. Bijnens, G. Ecker and J. Gasser, Nucl. Phys. B396 (1993) 81.
- [12] J. Wess and B. Zumino, Phys. Lett. 37B (1971) 95;
E. Witten, Nucl. Phys. B223 (1983) 422;
N.K. Pak and P. Rossi, Nucl. Phys. B250 (1985) 279.
- [13] G. Ecker, J. Gasser, A. Pich and E. de Rafael, Nucl. Phys. B321 (1989) 311;
G. Ecker, J. Gasser, H. Leutwyler, A. Pich and E. de Rafael, Phys. Lett. B223 (1989) 425;
J.F. Donoghue, C. Ramirez and G. Valencia, Phys. Rev. D39 (1989) 1947;
M. Praszalowicz and G. Valencia, Nucl. Phys. B341 (1990) 27.
- [14] V.N. Bolotov et al., Phys. Lett. B 243 (1990) 308.
- [15] A. Bay et al., Phys. Lett. B174 (1986) 445.
- [16] A.A. Poblaguev, Phys. Lett. B 238 (1990) 108.
- [17] V.M. Belyaev and I.I. Kogan, Phys. Lett. B 280 (1992) 238.
- [18] M.B. Voloshin, Phys. Lett. B 283 (1992) 120.

- [19] E. Gabrielli, Phys. Lett. B301 (1993) 409.
- [20] S. Krishna and H.S. Mani, Phys. Rev. D5 (1972) 678.
- [21] A.M. Diamant-Berger et al., Phys. Lett. 62B (1976) 485.
- [22] M.S. Atiya et al., Phys. Rev. Lett. 63 (1989) 2177.
- [23] S. Egli et al., Phys. Lett. B175 (1986) 97;
S. Egli et al., Phys. Lett. B222 (1989) 533.
- [24] J. Gasser and H. Leutwyler, Nucl. Phys. B250 (1985) 517.
- [25] N. Cabibbo and A. Maksymowicz, Phys. Lett. 9 (1964) 352.
- [26] H. Leutwyler and M. Roos, Z. Phys. C25 (1984) 91;
J.F. Donoghue, B.R. Holstein and S.W. Klimt, Phys. Rev. D35 (1987) 934.
- [27] Particle Data Group, Phys. Lett. B111 (1982).
- [28] G. Donaldson et al., Phys. Rev. D9 (1974) 2960.
- [29] V.K. Birulev et al., Nucl. Phys. B182 (1981) 1.
- [30] Y. Cho et al., Phys. Rev. D22 (1980) 2688.
- [31] D.G. Hill et al., Nucl. Phys. B153 (1979) 39.
- [32] A.R. Clark et al., Phys. Rev. D15 (1977) 553.
- [33] C.D. Buchanan et al., Phys. Rev. D11 (1975) 457.
- [34] L.-M. Chounet, J.-M. Gaillard and M.K. Gaillard, Phys.Rep. C4 (1972) 199.
- [35] E.P. Shabalin, Yad. Fiz. 49 (1989) 588 [Sov. J. Nucl. Phys. 49 (1989) 365]; ibid. 51 (1990) 464 [Sov. J. Nucl. Phys. 51 (1990) 296].
- [36] J. Bijnens and F. Cornet, Nucl. Phys. B296 (1986) 557.
- [37] S.R. Amendolia et al., Nucl. Phys. B277 (1986) 168 and references therein.
- [38] M.F. Heyn and C.B. Lang, Z.Phys. 7C (1981) 169;
N. Zovko, Forts. Phys. 23 (1975) 185.
- [39] R. Dashen and M. Weinstein, Phys. Rev. Lett. 22 (1969) 1337.
- [40] R. Dashen, L.-F. Li, H. Pagels and M. Weinstein, Phys. Rev. D6 (1972) 834.
- [41] B.G. Kenny, Phys. Rev. D15 (1977) 3481.

- [42] C.G. Callan and S.B. Treiman, Phys. Rev. Lett. 16 (1966) 153.
- [43] S.A. Akimenko et al., Phys. Lett. B 259 (1991) 225; for earlier works see [3].
- [44] J. Gasser and H. Leutwyler, Nucl. Phys. B250 (1985) 465.
- [45] B.R. Holstein, Phys. Rev. D41 (1989) 2829.
- [46] V.N. Bolotov et al., Yad. Fiz. 44 (1986) 108 [Sov. J. Nucl. Phys. 44(1986) 68].
- [47] F. Romano et al., Phys. Lett. 36B (1971) 525.
- [48] D. Ljung and D. Cline, Phys. Rev. D8 (1973) 1307.
- [49] K.J. Peach et al., Phys. Lett. 35B (1971) 351.
- [50] E. Fischbach and J. Smith, Phys. Rev. 184 (1969) 1645;
H.W. Fearing, E. Fischbach and J. Smith, Phys. Rev. D2 (1970) 542.
- [51] N. Cabibbo and A. Maksymowicz, Phys. Rev. 137 (1965) B438; erratum Phys. Rev. 168 (1968) 1926.
- [52] A. Pais and S.B. Treiman, Phys. Rev. 168 (1968) 1858.
- [53] L. Rosselet et al., Phys. Rev. D15 (1977) 574.
- [54] J. Bijnens, Nucl. Phys. B337 (1990) 635.
- [55] C. Riggensbach, J. Gasser, J.F. Donoghue and B.R. Holstein , Phys. Rev. D43 (1991) 127.
- [56] F.A. Berends, A. Donnachie and G.C. Oades, Phys. Lett. 26B (1967) 109; Phys. Rev. 171 (1968) 1457.
- [57] C. Riggensbach, University of Bern thesis (1992).
- [58] J.L. Basdevant, C.D. Froggatt and J.L. Petersen, Nucl. Phys. B72 (1974) 413.
- [59] C.D. Froggatt and J.L. Petersen, Nucl. Phys. B129 (1977) 89;
J.L. Petersen, CERN Yellow Report CERN 77-04 “The $\pi\pi$ Interaction”.
- [60] G.Makoff et al., Phys. Rev. Lett. 70 (1993) 1591.
- [61] M. Knecht, H. Sazdjian, J. Stern and N.H. Fuchs, Phys. Lett. B313 (1993) 229.
- [62] J. Bijnens, G. Colangelo, J. Gasser, BUTP-94/4, ROM2F 94/05, hep-ph/9403390, to appear in Nucl. Phys. B.
- [63] S. Weinberg, Phys. Rev. Lett. 17 (1966) 336; 18 (1967) 1178E.

- [64] J. Wess and B. Zumino, [12].
- [65] Ll. Ametller, J. Bijnens, A. Bramon and F. Cornet, Phys. Lett. B303 (1993) 140.
- [66] J. Donoghue, J. Gasser and H. Leutwyler, Nucl. Phys. B343 (1990) 341.
- [67] T.N. Truong, Phys. Rev. Lett. 61 (1988) 2526; Phys. Lett. 99B (1981) 154.
- [68] A.D. Martin and T.D. Spearman, Elementary particle theory (North-Holland, Amsterdam, 1970).
- [69] M. Knecht, B. Moussallam and J. Stern, Orsay-preprint IPNO/TH 94-08 (hep-ph/9402318).
- [70] MINUIT Reference Manual, Application Software Group, Computing and Network Division, CERN.
- [71] M.M. Nagels et al., Nucl. Phys. B147 (1979) 189.
- [72] A. Schenk, Nucl. Phys. B363 (1991) 97.
- [73] T.N. Pham and T.N. Truong, Phys. Rev. D31 (1985) 3027.
- [74] J. Stern, H. Sazdjian and N.H. Fuchs, Phys. Rev. 47 (1993) 3814.
- [75] For a proposal to measure $\pi\pi$ and πK threshold parameters in dimeson atoms see L. Montanet and L. Nemenov, Letter of Intent to the SPSLC, CERN/SPSLC 91-47.
- [76] G. Makoff, private communication.
- [77] J. Gasser and H. Leutwyler, Ann. Phys. 158 (1984) 142.
- [78] J. Gasser and H. Leutwyler, Phys. Lett. B125 (1983) 321, 325.
- [79] S. Weinberg, Phys. Rev. Lett. 17 (1966) 616.
- [80] B. Bonnier and N. Johanneson, Nuovo Cimento 29A (1975) 565.
- [81] J. Franklin, Phys. Rev. D11 (1975) 513.
- [82] M. Gell-Mann, R.J. Oakes and B. Renner, Phys. Rev. 175 (1968) 2195.
- [83] M. Knecht and J. Stern, Generalized chiral perturbation theory, this Handbook.
- [84] G. Colangelo, Paula J. Franzini, M. Knecht, J. Stern, this report.
- [85] S. Blaser, Diploma thesis, Bern University, 1994.